Cell Reports

Article

Structural basis of interleukin-17B receptor in complex with a neutralizing antibody for guiding humanization and affinity maturation

Graphical abstract

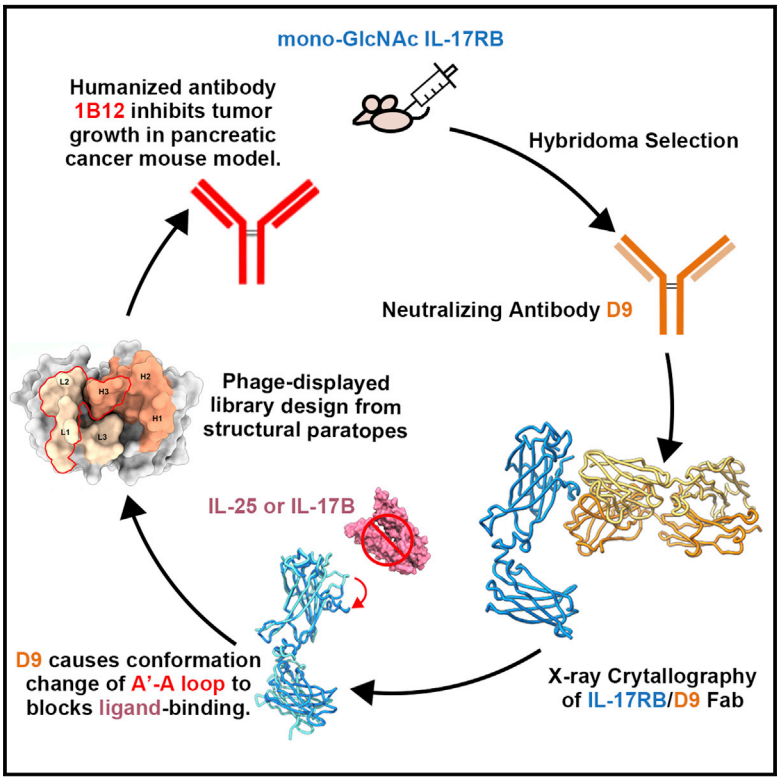

Highlights

- Mono-GlcNAc IL-17RB is used as an immunogen for generating neutralizing antibodies
- A conformational change by antibody D9 binding leads to inhibiting IL-17RB pathway
- Structure of D9-bound IL-17RB guides the affinity maturation of humanized antibodies
- Affinity-matured humanized antibody 1B12 is obtained with good anti-cancer activity

Authors

Wen-Hsin Lee, Xiaorui Chen, I-Ju Liu, ..., Sheng-Kai Wang, Wen-Hwa Lee, Che Ma

Correspondence

whlee@uci.edu (W.-H.L.), cma@gate.sinica.edu.tw (C.M.)

In brief

Lee et al. report the X-ray crystal structure of IL-17RB in complex with the Fab of a neutralizing antibody revealing the detailed atomic view of the inhibitory mechanism for IL-17RB signaling pathways. From the structural information, a humanized antibody 1B12 against IL-17RB is produced and inhibits tumor growth *in vivo*.

Lee et al., 2022, Cell Reports *41*, 111555
October 25, 2022 © 2022 The Authors.
https://doi.org/10.1016/j.celrep.2022.111555

CellPress

Cell Reports

CellPress
OPEN ACCESS

Article

Structural basis of interleukin-17B receptor in complex with a neutralizing antibody for guiding humanization and affinity maturation

Wen-Hsin Lee,[1,2,3] Xiaorui Chen,[1] I-Ju Liu,[6] Jiin-Horng Lee,[1] Chun-Mei Hu,[1] Han-Chung Wu,[6,7] Sheng-Kai Wang,[3] Wen-Hwa Lee,[1,4,5,*] and Che Ma[1,2,8,*]

[1]Genomics Research Center, Academia Sinica, Taipei, Taiwan
[2]Chemical Biology and Molecular Biophysics, Taiwan International Graduate Program, Academia Sinica, Taipei, Taiwan
[3]Department of Chemistry, National Tsing Hua University, Hsinchu, Taiwan
[4]Department of Biological Chemistry, University of California, Irvine, Irvine, CA, USA
[5]Drug Development Center, China Medical University, Taichung, Taiwan
[6]Institute of Cellular and Organismic Biology, Academia Sinica, Taipei, Taiwan
[7]Biomedical Translation Research Center (BioTReC), Academia Sinica, Taipei, Taiwan
[8]Lead contact
*Correspondence: whlee@uci.edu (W.-H.L.), cma@gate.sinica.edu.tw (C.M.)
https://doi.org/10.1016/j.celrep.2022.111555

SUMMARY

Upregulation of interleukin-17 receptor B (IL-17RB) is known to be oncogenic, while other IL-17 receptors and ligands are generally involved in pro-inflammatory pathways. We identify a mouse neutralizing monoclonal antibody (mAb) D9, which blocks the IL-17RB/IL-17B pathway and inhibits pancreatic tumorigenesis in an orthotopic mouse model. The X-ray crystal structure of the IL-17RB ectodomain in complex with its neutralizing antibody D9 shows that D9 binds to a predicted ligand binding interface and engages with the A′-A loop of IL-17RB fibronectin III domain 1 in a unique conformational state. This structure also provides important paratope information to guide the design of antibody humanization and affinity maturation of D9, resulting in a humanized 1B12 antibody with marginal affinity loss and effective neutralization of IL-17B/IL-17RB signaling to impede tumorigenesis in a mouse xenograft model.

INTRODUCTION

Cytokines and receptors of the interleukin (IL)-17 superfamily govern the inflammatory pathways in both adaptive and innate immune responses, in which the IL-17 ligand/cytokine is secreted by T helper 17 (Th17) cells and recognized by IL-17 receptors (IL-17Rs) on various types of cells for downstream signaling (Gaffen, 2009; Harrington et al., 2005; Park et al., 2005). This family includes six ligand members from IL-17A to IL-17F and five receptor members, IL-17 receptor A through E, and the combinations of different ligands and receptors can lead to different signaling pathways and physiological consequences (Gaffen, 2009; McGeachy et al., 2019). For example, IL-17A and IL-17F share the same receptor IL-17RA and induce the Th17-driven inflammation in keratinocytes, contributing to several skin syndromes (Brembilla et al., 2018; Zwicky et al., 2020). IL-17B and IL-17E (also known as IL-25) share the same receptor IL-17RB, but play different roles in pro-inflammation signaling, including neutrophil recruitment by IL-17B in the intestine and upregulation of type 2 immunity related cytokines by IL-17E in mucosal system related asthma, respectively (Swaidani et al., 2009). IL-17C and IL-17D can promote innate immune response to defend pathogens in endothelial cells (McGeachy et al., 2019).

All IL-17 receptors contain at least two extracellular fibronectin type III (FnIII) domains, a single transmembrane helix, and a cytoplasmic SEFIR domain (similar expression to fibroblast growth factor genes and IL-17R) for downstream signaling (Gaffen, 2009; Liu, 2019; McGeachy et al., 2019). Among them, IL-17RA plays a central role in autoimmunity via TRAF6-mediated activation of NF-kappa-B and MAP kinase pathways (Maitra et al., 2007), and extensive efforts have been put in the development of therapeutic antibodies targeting IL-17RA to attenuate its signal transduction (Adams et al., 2020; Papp et al., 2012). Another member IL-17RB (also known as IL-17Rh1, IL-25R, or Evi27) shares only 14.8% sequence identity with IL-17RA and has become increasingly significant due to its recently discovered role in cancer progression (Bie et al., 2016; Gelaleti et al., 2017; Huang et al., 2014, 2017; Laprevotte et al., 2017; Vitiello and Miller, 2020; Wu et al., 2015; Yang et al., 2018). In addition, the IL-17RA/B heterodimer plays critical roles in the initiation and propagation of Th2-type immune response through their ligand IL-17E (IL-25) acting on type II innate lymphoid cells (ILC2) to provide protection from parasitic worms or helminths in the intestine (Barlow and McKenzie, 2009).

We have recently found that IL-17RB homodimers can recruit mixed-lineage kinase 4 (MLK4) to phosphorylate its SEFIR

This is an open access article under the CC BY-NC-ND license (http://creativecommons.org/licenses/by-nc-nd/4.0/).

domain, promoting cancer progression and metastasis through the ERK1/2 pathway (Wu et al., 2021). Moreover, the upregulation of IL-17RB can enhance IL-17B expression in positive autocrine feedback, leading to a worsened prognosis in pancreatic cancer patients as well as the resistance to paclitaxel treatment in breast tumors (Huang et al., 2014, 2017; Laprevotte et al., 2017; Wu et al., 2015). We also reported an IL-17-RB-neutralizing monoclonal antibody D9 that could block IL-17RB/IL-17B pathways and inhibit pancreatic tumorigenesis in an orthotopic mouse model (Wu et al., 2015), reinforcing the idea that an IL-17RB antagonist could be developed for treating pancreatic cancers. While several antagonists of the IL-17RA/IL-17A signaling pathway are clinically available, such as human mAb brodalumab, secukinumab, and humanized ixekizumab, bimekizumab for treating psoriasis and psoriatic arthritis (Adams et al., 2020; Armstrong and Read, 2020), no similar drugs have yet been developed for IL-17RB. One knowledge gap lies in the lack of a detailed understanding of the molecular recognition between IL-17RB and its targeting antibody at the atomic level.

In this study, we described the specific deglycosylation strategy during the identification of D9 antibody. We further solved the X-ray crystal structure of D9 Fab domain in complex with bovine IL-17RB ectodomain. Compared with the ligand-bound structures of IL-17RB, IL-17RA, and IL-17RC, our structure reveals how ligand binding could modulate the arrangement of extracellular FnIII domains of the IL-17R receptors. The structure shows the detailed binding interface between IL-17RB and D9 antibody, which proposes the mechanism of neutralization by D9 and provides a structural basis for guiding the humanization and affinity maturation of D9. The affinity-matured humanized antibody clone 1B12 was identified and it demonstrated significant inhibition of pancreatic tumorigenesis in an orthotopic mouse model.

RESULTS

Identification of the neutralizing monoclonal antibody D9 from mice immunized with mono-GlcNAc decorated IL-17RB

To generate mouse monoclonal antibody against human IL-17RB (hIL-17RB), we prepared the mono-GlcNAc decorated hIL-17RB ($IL\text{-}17RB_{MG}$) as the immunogen to compare with the original fully glycosylated protein ($IL\text{-}17RB_{FG}$), based on our previous reports that removal of the glycan shield could elicit higher immune response in mice (Chen et al., 2014; Huang et al., 2022). We expressed the extracellular domain (R18 to P292, extracellular domain [ECD]) of hIL-17RB in human embryonic kidney 293S cells (HEK293S), which lack N-acetylglucosaminyltransferase I ($GnTI^{-}$) and can only produce glycoproteins decorated with high-mannose-type (HM) glycans, mainly $Man_5GlcNAc_2$ (Man-5) (Reeves et al., 2002). The HM glycans were enzymatically trimmed by Endoglycosidase-H to a single N-acetylglucosamine (GlcNAc) on each N-glycosite of IL-17RB (N67, N103, N156, N183, N197, and N283), generating the $IL\text{-}17RB_{MG}$ protein. On the other hand, $IL\text{-}17RB_{FG}$ was purified from HEK293 EBNA cells carrying the close-to-native glycoforms (Figure 1A). Both $IL\text{-}17RB_{MG}$ and $IL\text{-}17RB_{FG}$ were treated with Tobacco Etch Virus (TEV) protease to remove the C-terminal affinity tag to prevent nonspecific immune responses in mice. While the immunization did not affect the body weight of mice, the IL-17RB-specific serum immunoglobulin (Ig)G titer was found to be significantly higher in the $IL\text{-}17RB_{MG}$ group than $IL\text{-}17RB_{FG}$ (Figure 1B). Several highly potent antibodies were identified from the hypoxanthine-aminopterin-thymidine (HAT)-selected hybridoma clones of the $IL\text{-}17RB_{MG}$ immunized mice, using ELISA and flow cytometry to screen for cells with double-positive hIL-17RB-EGFP and anti-mouse Cy5 signals (Figure 1C). These positive clones were further tested by soft agar colony formation assay and only D9 was confirmed with tumorigenesis-inhibiting activity (Figure 1D).

Overall structure of bIL-17RB in complex with D9 Fab

The cDNA that encodes the variable region of mouse neutralizing monoclonal D9 antibody (mD9) was cloned into a human IgG1 expression vector, generating the chimeric antibody D9 (cD9). Antibody cD9 was recombinantly purified and papain-digested into the Fab fragment for crystallization in complex with IL-17RB ECD. For the structural study, we chose bovine IL-17RB (bIL-17RB) for its high yield and purity, as the human homologue (hIL17-RB) had a much lower yield and failed to crystallize, while the two exhibited comparable binding avidities with mD9 (Figure S1). The 2.19Å resolution crystal structure of the bIL-17RB/cD9-Fab complex revealed two proteins in a stoichiometry of 1:1, with four copies of the complex in one asymmetric unit (Figures S2A and S2B and Table 1). The initial molecular replacement solution only resulted in four Fab structures and three IL-17RB, while the remaining copy of IL-17RB was built manually. Interestingly, these four copies of IL-17RB in the asymmetric unit do not superimpose well, revealing a significant difference in structural orientation, which is possibly attributed to the impact of crystal packing and its intrinsic flexibility (Figure S2C).

The overall folding of IL-17RB is very similar to that of IL-17RA (Figures 2B and 2C), although the extracellular region of bovine IL-17RB and human IL-17RA share relatively low sequence identity (23.5%, Figure S3A). The bIL-17RB contains two fibronectin type III (FnIII) domains, D1 and D2, joined by a 20-amino-acid linker (Figure 2A). Each domain folds into two antiparallel β-sheets to form a stable double-layer β-sandwich structure, which is held by hydrophobic interactions as well as disulfide bonds and further covered by N-glycans (Figures S3B and S3C and S4C and S4D). To date, there are four available structures of IL-17RA ECD, which are PDB: 3JVF (in complex with IL-17F homodimer) (Ely et al., 2009), PDB: 4HSA (in complex with IL-17A homodimer) (Liu et al., 2013), PDB: 5NAN (in complex with IL-17A/F heterodimer) (Goepfert et al., 2017) and PDB: 5N9B (by A. Goepfert et al.; unligand ECD), one structure of IL-17RC, PDB: 6HG4 (in complex with IL-17F), and notably the recently reported cryo-EM structures of IL-17RB, PDB: 7UWL, 7UWJ, 7UWK (Wilson et al., 2022). We superimposed the D1 or D2 domain from each of these IL-17 receptors onto our IL-17RB structure and found that they are structurally conserved (the root-mean-square deviation [RMSD] of D1 up to 1.232 Å; RMSD of D2 up to 1.963 Å) (Figures 2B–2E). However, between the liganded and unliganded IL-17RA structures we observed a 7.2 Å shift of D2 when only D1 was superimposed, indicating that the two FnIII domains are closer when the ligand is absent

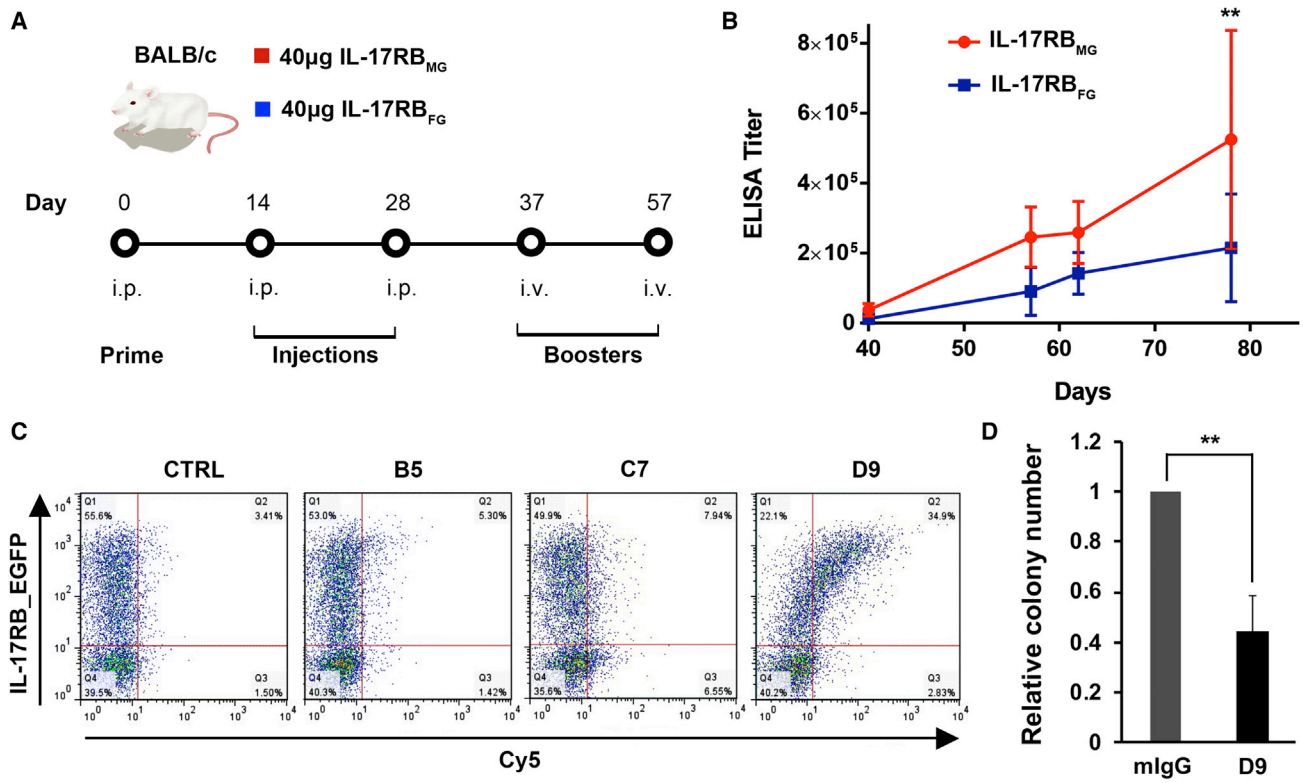

Figure 1. Identification of the neutralizing mAb D9 from mice immunized by mono-GlcNAc decorated (MG) IL-17RB$_{MG}$

(A) Schematic view of the experimental design. The mono-GlcNAc decorated (MG) or fully glycosylated (FG) IL-17RB ECD proteins were intraperitoneally injected into female BALB/c mice (n = 6) with one prime boost at day 0, two injections with adjuvant Al(OH)$_3$ for a 2-week interval, followed by two intravenous boosters.

(B) ELISA titer of the serum from the immunized mice against hIL-17RB over time. The IL-17RB$_{MG}$ group elicited significantly higher ELISA titer than the IL-17RB$_{FG}$ group (one-way ANOVA, $p < 0.001$).

(C) The flow cytometry results of double-positive (EGFP and Cy5) signals of different hybridoma monoclonal antibody clones (B5, C7, and D9) and the control (CTRL).

(D) The soft agar colony formation assay (SACF) of D9 tested for pancreatic cancer cell line CFPAC-1, using mouse normal IgG as control (n = 6). Data are means ± SD in three technical replicates. **$p < 0.001$ by one-way ANOVA analysis. All statistics were analyzed by Prism.

(Figure S4B). Interestingly, the D9-Fab-bound IL-17RB structure exhibits an even larger shift of D2, for up to ~34 Å in distance and ~50° turning toward D1, compared with all the other ligand-bound receptors (Figure 2F). This orientation of D2 is strengthened with a hydrogen bond between S45-O_γ on the A-B loop and K153-N_ζ on the linker (Figure S4A), which can occur only when the A-B loop flips toward D2, with an ~14 Å deviation compared with that of IL-17RA (Figure S4B). The different degrees of D2 bending found in four symmetry mates also suggested a structural flexibility of the hinge region between D1 and D2 (Figure S2C), and the ligand-free IL-17 receptors may have the potential to adopt a different conformation that was unrealized before. Under this hypothesis, the flexible D1-D2 linker would open up the space between of two FnIII domains to accommodate the binding ligand, as shown in the extended structural arrangement of D1 and D2 in the structures of IL-17RA and IL-17RC in complex with ligands, but not in the two apo structures of IL-17RA (PDB: 5N9B) and IL-17RB as in this study.

In addition, the structural location of disulfide bonds in IL-17RB is similar to that of IL-17RA in the D2 domain but different in D1, which may stabilize different structural elements and indirectly affect ligand binding (Figure S4A). The distribution pattern of N-glycosites of IL-17RB is also very different from that of IL-17RA, which may lead to different ligand binding behaviors between the two receptors (Figure S4D). Finally, the N-terminal loop of IL-17RB is 14 amino acids shorter than that of IL-17RA (UniProt, 2021), yet without affecting the overall folding of D1 domain (Figures S3A–S3C). This loop is related to the first disulfide bond of both proteins (C12-C19 in IL-17RA and C7-85 in IL-17RB) and may alter the local environment of surrounding side chains.

A unique conformational state of IL-17RB upon D9 binding

The most unusual feature of the IL-17RB/D9 complex structure is the A′-A loop that adopts a dramatically different conformation as compared with the structure of all the other IL-17 receptors (Figures 2B–2D). This loop is the primary site for D9 interaction, which comprises 20 residues from P11 to D30, including several highly conserved residues with IL-17RA, such as W17, L23, P25, D30, and L31 (Figure S3A). The superimposition of IL-17RB/IL-

Table 1. Data collection and refinement statistics of bIL-17RB-ECD/cD9-Fab complex

Data collection	
Space group	P1 $2_1$1
Total reflections	268,478 (26,679)
Unique reflections	134,260 (13,343)
Cell dimensions	
a, b, c (Å)	70.02, 195.03, 98.83
α, β, γ (°)	90.00, 98.13, 90.00
Wavelength (Å)	1.07
Resolution (Å)	38.03–2.19 (2.268–2.19)
Completeness	99.95% (99.97%)
Redundancy	2.0 (2.0)
R_{merge}	0.095 (0.725)
I/σI	7.08 (1.59)
$CC_{1/2}$	0.996 (0.557)
Solvent content	42.01% (four complexes in one asymmetry unit)
Refinement statistics	
Reflections (Total/Test)	134,224 (13,339)
R_{factor}/R_{free} (%)	19.13/23.74
Atoms	
Protein	2,717
Carbohydrate	29
Solvent	1,021
Root-mean-square deviations	
Bond length (Å)	0.008
Bond angle (Å)	1.06
Mean B value (Å^2)	45.90
Ramachandran favored (%)	95.80
Ramachandran allowed (%)	4.02
Ramachandran outliers (%)	0.19

25 and IL-17RB/D9 structures revealed a clash between this A′-A loop and the binding ligand IL-25 (Figures 3A and 3B). As the tracing of the D9-bound A′-A loop is justified by clear electron densities, its distinct conformation as winding underneath the F-G loop is confident and unexpected (Figure 3C). To investigate the relationship between this conformational state and ligand recognition, we mapped the ligand-interacting residues of IL-17RA with IL-17A homodimer, IL-17F homodimer, or IL-17A/F heterodimer (Figure 3D), and colored them in a heat map based on their structural conservation (Figure 3E). We then hypothesized that ligand interaction of IL-17RB is homologous to that of IL-17RA and mapped the corresponding residues as the potential ligand binding site of IL-17RB (Figure 3F), because the ligand/receptor interaction mode and the interface residues are highly conserved within the IL-17 family (Ely et al., 2009; Goepfert et al., 2017; Liu et al., 2013). Particularly, the key residue W31 of IL-17RA is in the ligand binding pocket and its mutant W31A completely lost the binding activity of IL-17A (Liu et al., 2016). However, in our IL-17RB/D9 Fab structure, this tryptophan (corresponding to W17 in IL-17RB) shifts dramatically from facing outward to inward, making it impossible to engage with any ligand (Figure 3G). More importantly, the A′-A loop structurally overlaps with the potential ligand recognition site based on IL-17RA structures (Figure 3G), as well as with the reported IL-25-binding site in the cryo-EM structure od IL-17RB (Figure 3H). Such a conformational shift of the A′-A loop will result in a substantially altered binding surface of IL-17RB, suggesting that the same binding mode of the ligand would be hardly possible when D9 is bound. While it remains to be confirmed whether this is an induced fit by D9 or D9 only helps stabilize one of the many flexible conformation states, these findings have provided key insights into the inhibitory mechanism of D9 that its interaction with the A′-A loop would block the natural ligand binding site, prevent the ligand-driven dimerization of IL-17RB, and disable the downstream signaling cascades of IL-17B/IL-17RB in cancer progression (Figure 3I) (Wilson et al., 2022; Wu et al., 2021).

Detailed interface between IL-17RB and D9 antibody

The interaction between IL-17RB and D9 antibody uses the residues mostly from CDR3 of the light chain (LCDR3) with only a few residues of light chain CDR1 (LCDR1) and CDR2 and CDR3 of the heavy chain (HCDR2/3) (Figure 4A). D9 primarily contacts the A′-A loop of IL-17RB D1, from residue P11 to D30, with a buried interface area of around 1492Å^2. Near the C-terminus of the A′-A loop, R29 of IL-17RB forms salt bridges with LCDR2-D49 of D9, and the adjacent D30-$O_{\delta2}$ makes a polar contact with the hydroxyl group of LCDR1-Y30. Both and LCDR1-Y30 are further stabilized by parallel guanidinium/aromatic stacking with HCDR3-Y101 of D9 and R56 of IL-17RB, respectively (Figure 4B). Near the center of the binding pocket, a hydrogen bond network is observed involving LCDR1-Y31-O, LCDR3-W90-N, LCDR3-S91-O_γ of D9, and D27-$O_{\delta2}$ of IL-17RB, which are coordinated by a water molecule, further connected with LCDR1-H33-$N_{\varepsilon2}$ and HCDR3-G102-N via D27 (Figure 4C). At the middle part of the A′-A loop, P25 of IL-17RB and LCDR3-W90 of D9 form a CH/π stacking (Figure 4D), with the nearby LCDR3-N93-$N_{\delta2}$ interacting with L23-O of IL-17RB. Interestingly, HCDR2-N55-$N_{\delta2}$ interacts with O6 of the N-GlcNAc on N139, the glycosite that is located very closely to the predicted ligand binding site (Figure 4E). Moreover, we also aligned the A′-A loop sequences of human and bovine IL-17RB and found there are two different amino acids at positions 22 and 24, which are D22 and I24 in human but T22 and T24 in bovine (Figure S3A). The observed polar contact between T22-O_γ HCDR2-T59-O_γ may not be affected by the T22D substitution, as both side chains are similar in size and capable of forming the hydrogen bond. And T24 is not involved in any interaction with D9 antibody. Therefore, the result shown by the bovine IL-17RB structure could be representative to illustrate the interface between human IL-17RB and D9 antibody and to provide guidance for functional studies as follows.

Paratope of antibody D9 and functional analysis

To evaluate the functional contribution of each complementarity-determining region (CDR) residue in the D9 paratope that interacts with IL-17RB, we used alanine-scanning mutagenesis and measured the binding activity of each antibody mutant. From

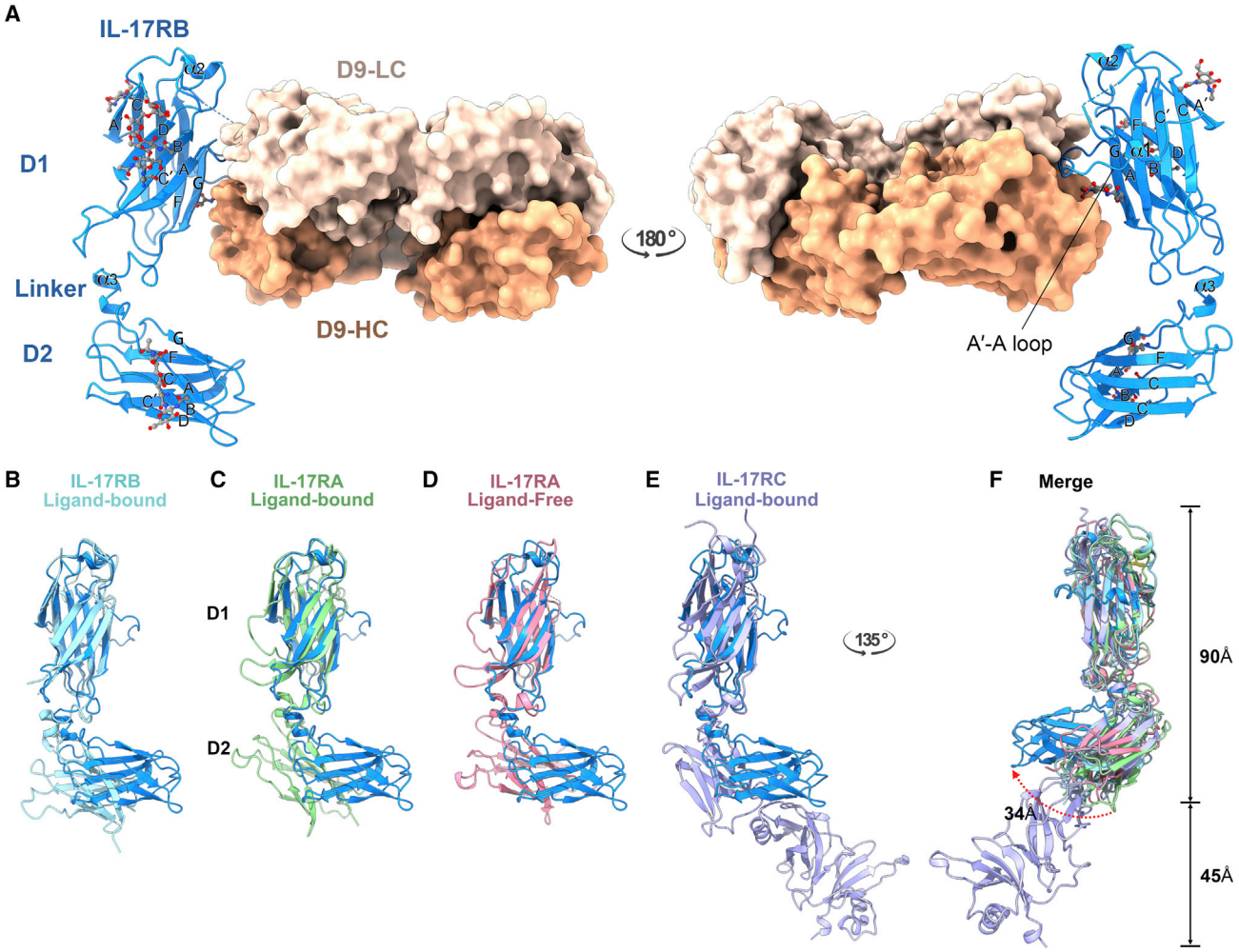

Figure 2. Structure of IL-17RB in complex with D9-Fab and the superimposition with other IL-17 receptors

(A) The overall complex structure of the bovine IL-17RB ECD (bIL-17RB; cartoon presentation in blue) and D9 Fab (surface presentation; light chain in light orange; heavy chain in orange) are shown in two views with 180° rotation. Fibronectin type III domain 1 (D1), D2, the D1-D2 linker, and all secondary structural elements are labeled. The A′-A loop that is recognized by D9 is highlighted. N-glycans are shown in the stick-ball mode with C atoms colored in gray.

(B–E) Superimposed structures of bIL-17RB with four IL-17 receptors on their D1 domains, including the ligand-bound hIL-17RB (B, colored in cyan, PDB: 7uwl), ligand-bound IL-17RA (C, colored in green, PDB: 3JVF), the ligand-free hIL-17RA (D, colored in pink, PDB: 5N9B), and the ligand-bound hIL-17RC (E, colored in purple, PDB:6HG4).

(F) Four superimposed structures with a 135-degree right rotation from (B–E). The D2 of IL-17RB exhibits a different orientation when compared with hIL-17RA and hIL-17RC, showing a shift for ~34Å and a rotation for ~50° toward D1.

the ELISA results, D9 mutants of HCDR3-G102A, Q88A, Q89A, W90A, S91A, N93A, and LCDR3-P94A all exhibited decreased binding toward human IL-17RB (Figure 5A), while mutating other interacting residues on HCDRs, LCDR1, and LCDR2 had a minimal impact. It is noteworthy that the decreased binding observed for LCDR1-S91A mutant could be attributed to the interaction between LCDR1-S91-O_γ and LCDR3-Y30-N, which stabilizes the conformation of two CDR loops (Figure 4B). So are the results of LCDR3-Q88A and HCDR3-G102A mutants that these two residues help to hold the conformation of LCDR3, which is crucial for IL-17RB binding (Figure 4C). We further mapped the structurally interacting CDR residues on the D9 Fab structure in parallel with the key functional residues (>80% binding loss from alanine-scanning results) and found that the most important interactions are through LCDR3 at the innermost center of the paratope (Figures 5B–5D). This region appears like a flat "U"-shape platform to attract, distort, and stabilize the A′-A loop mainly through backbone hydrogen bonding and CH/π stacking.

Humanization and affinity maturation of antibody D9

The combination of structural and functional information of the IL-17RB/D9 interface has provided us with an invaluable guidance for generating therapeutically useful anti-hIL-17RB antibodies. First, we engrafted the CDRs of D9 into the framework of the commercialized anti-human epidermal growth factor receptor 2 (HER2) antibody, Trastuzumab, with the human IgG1

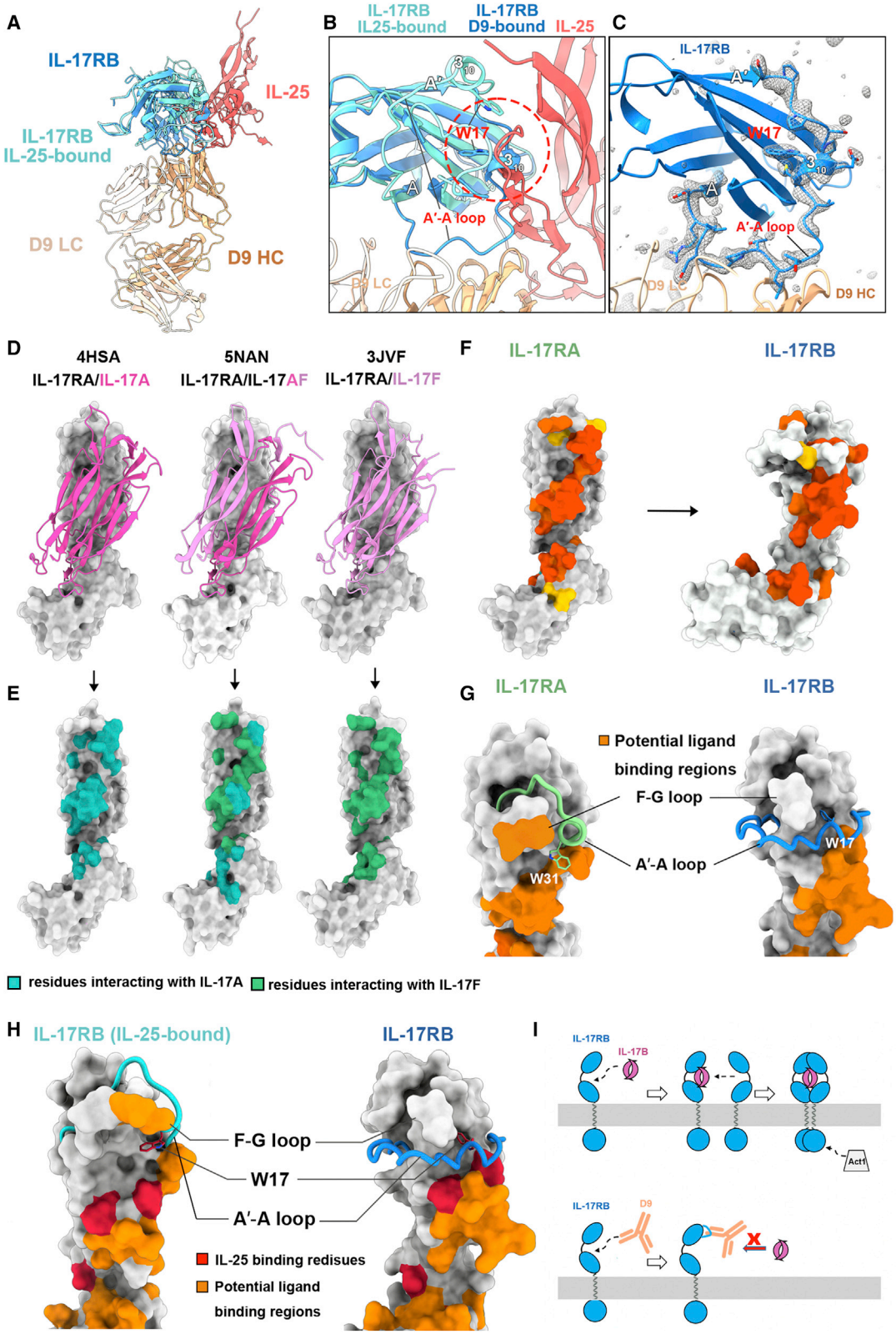

(legend on next page)

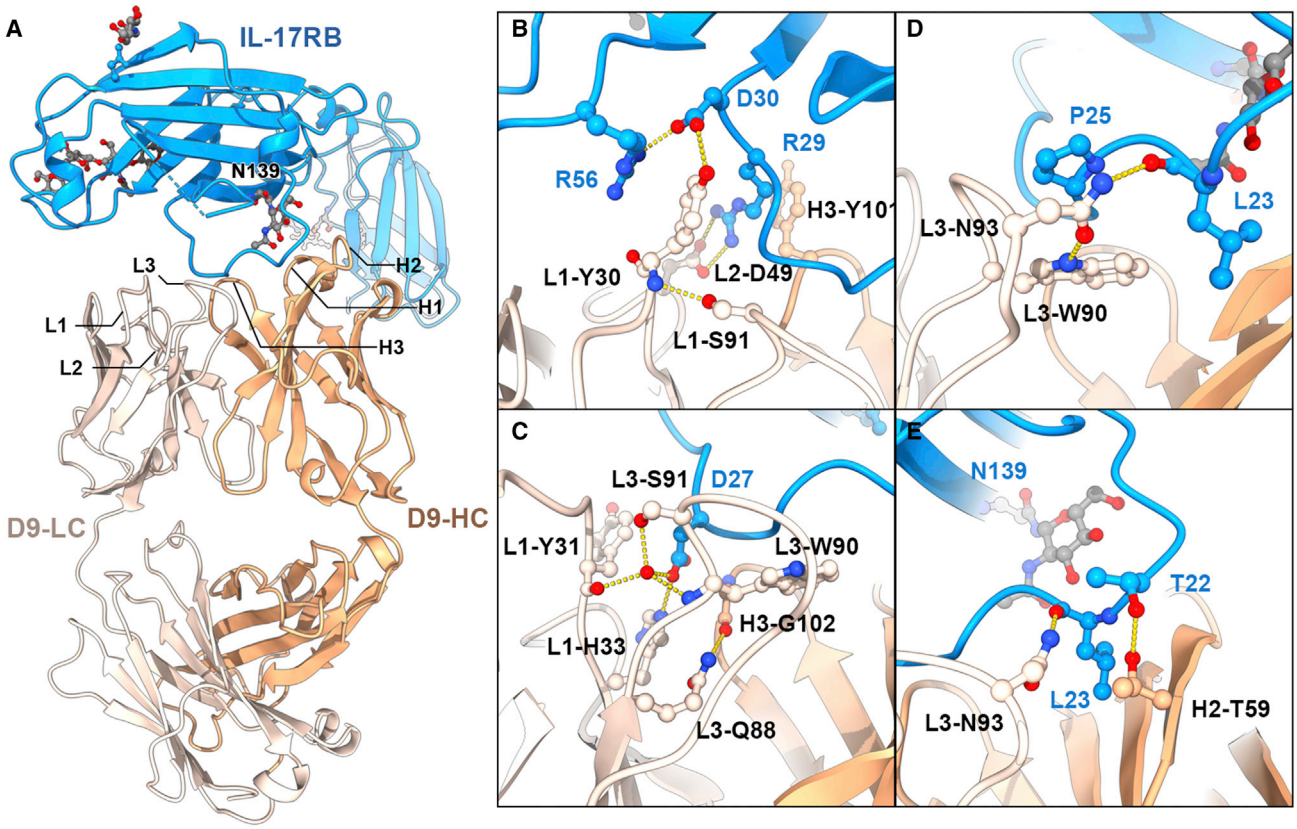

Figure 4. Detailed interface between IL-17RB and the complementarity-determining regions (CDRs) of D9

(A) The overall view of D9 CDRs interacting with IL-17RB, colored as in Figure 1 (IL-17RB: blue, D9 heavy chain: orange, light chain: light orange). CDRs are labeled as H1, H2, and H3 (heavy chain) and L1, L2, and L3 (light chain). N-glycans are shown in gray sticks. One N-glycosite in the interface (N139) is labeled.

(B–E) Enlarged views of the interface between IL-17RB and D9 showing the C-terminal part of the A′-A loop (B), the near C-terminal part (C), the near N-terminal part (D), and the N-terminal part (E) in interaction with D9 CDRs. The contact residues are drawn in stick-ball mode, colored according to molecules. Hydrogen bonds are drawn as yellow dashed lines. Water molecules in red spheres. The N-glycan in gray sticks. D9 residues are labeled with their location (e.g., H1 for HCDR1) included.

constant fragment (Fc). This humanized D9 (hD9) can still bind to hIL-17RB with a K_D of 35 nM compared with the original mD9 with a K_D of 11 nM by biolayer interferometry (BLI) measurements (Figure S5). We further confirmed that bovine and human IL-17RB share the same binding epitope to both mD9 and hD9 by phage-displayed random peptide library assay (Figures S6A–S6C) and found four of random peptide sequences with dose-dependent binding that were identical between the two groups (Figure S6D). To increase the binding affinity of the humanized D9 and retain the high neutralization potency as

Figure 3. The A′-A loop of IL-17RB adopts a unique conformation in complex with D9

(A) The D9-bound-bIL-17RB structure is superimposed with the IL-25-bound hIL-17RB (PDB: 7uwj), colored by molecules (D9-bound-bIL-17RB: blue, IL-25-bound-IL-17RB: cyan, D9: light orange, IL-25: salmon).

(B) An enlarged view of (A) shows a crash between IL-25 and the A′-A loop (red dashed circle) in the superimposed structures. The ligand binding residue W17 is highlighted in sticks and labeled.

(C) The electron density map of the A′- A loop of D9-bound-bIL-17RB at 1.0 σ contour shown in a gray mesh.

(D) Structure of IL-17RA in complex with either the dimeric IL-17A (PDB code: 4HSA) or with the heterodimeric IL-17A/F (PDB code: 5NAN) or with the dimeric IL-17F (PDB code: 3JVF). IL-17RA shown in gray surface, IL-17A in pink, and IL-17F in light pink.

(E) Mapping of interacting residues with IL-17A (colored in cyan) or IL-17F (colored in green) on IL-17RA based on (D).

(F) Heat map of the combined interacting residues on IL-17RA (left). Yellow: interacting with one ligand; dark orange: with two ligands; red: with all ligands. Corresponding residues were mapped on IL-17RB as the potential ligand binding site (right).

(G) The position of the A′- A loop of IL-17RA (green) and IL-17RB (blue) relative to the potential ligand binding site (dark orange) as in (F). W17/W31 are highlighted in sticks.

(H) The position of the A′- A loop (licorice mode, colored as in A) relative to the IL-25 binding-residues (red) and the predicted ligand binding site (dark orange).

(I) A simplified model of the inhibitory mechanism of D9. Without D9, the dimerized ligand IL-17B binds to the monomeric IL-17RB and induces the dimerization of IL-17RB for downstream signal transduction. When D9 is present, it interacts with the A′-A loop of IL-17RB and blocks its interaction IL-17B to inhibit adaptor Act1 signaling cascade.

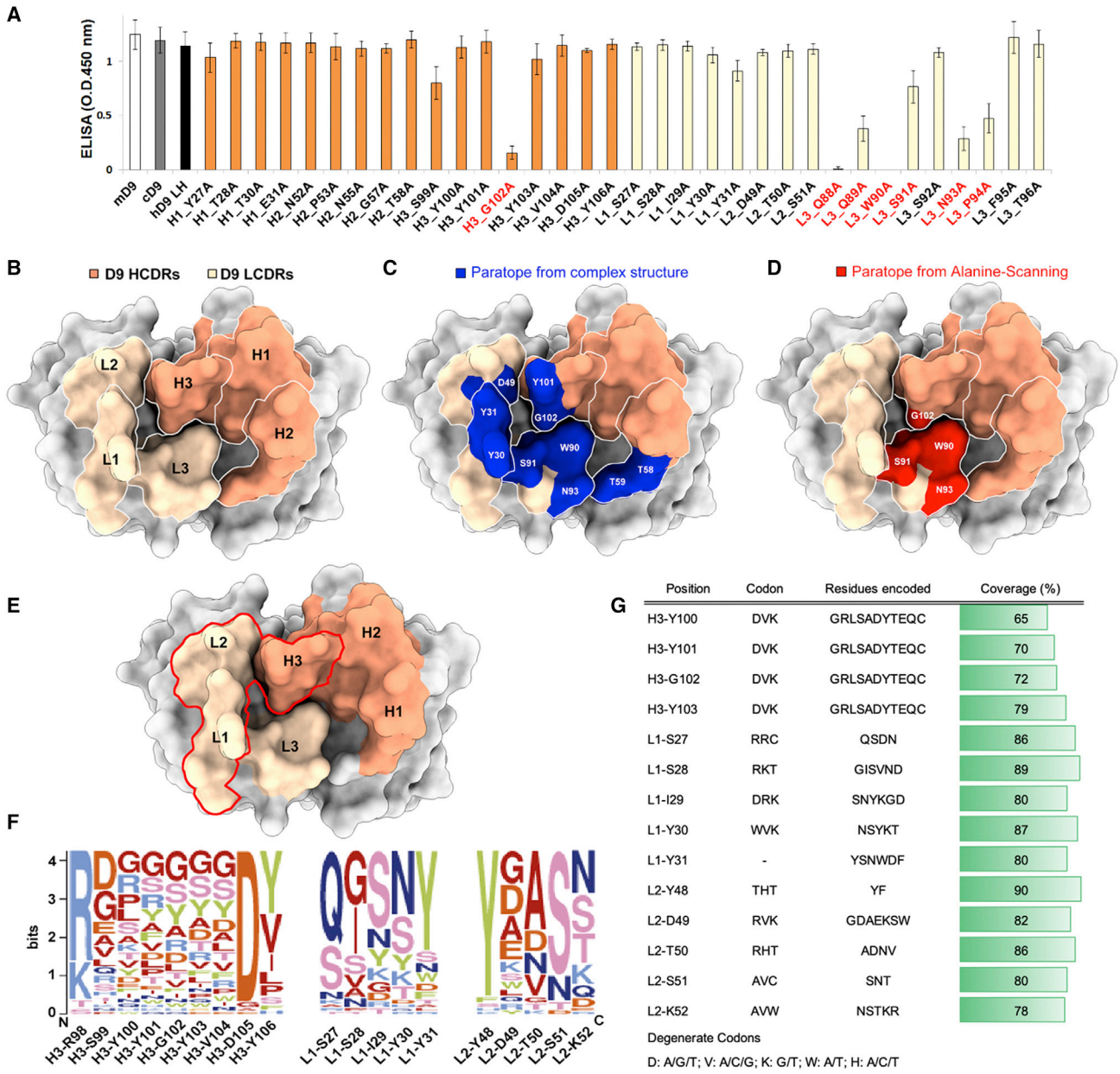

Position	Codon	Residues encoded	Coverage (%)
H3-Y100	DVK	GRLSADYTEQC	65
H3-Y101	DVK	GRLSADYTEQC	70
H3-G102	DVK	GRLSADYTEQC	72
H3-Y103	DVK	GRLSADYTEQC	79
L1-S27	RRC	QSDN	86
L1-S28	RKT	GISVND	89
L1-I29	DRK	SNYKGD	80
L1-Y30	WVK	NSYKT	87
L1-Y31	-	YSNWDF	80
L2-Y48	THT	YF	90
L2-D49	RVK	GDAEKSW	82
L2-T50	RHT	ADNV	86
L2-S51	AVC	SNT	80
L2-K52	AVW	NSTKR	78

Degenerate Codons
D: A/G/T; V: A/C/G; K: G/T; W: A/T; H: A/C/T

Figure 5. Paratope residues of D9 antibody analyzed by alanine scanning and the design of hD9 affinity maturation

(A) The ELISA result of the alanine-scanning mutant of each D9 CDR residue. Red labels highlight the residues with a substantial reduction in the binding to IL-17RB. Bars are colored accordingly (heavy chain: orange, light chain: light orange).

(B) The surface presentation of D9 Fab showing all the CDRs, colored as in (A).

(C and D) The paratope of D9 as observed in crystal structure (C, in dark blue) and key functional residues from alanine-scanning results (D, in red) are mapped on the D9 Fab structure as in B.

(E) The position of H3, L1, and L2 is highlighted in red contour line.

(F) The natural diversity of each amino acid on H3, L1, and L2.

(G) The CDR randomized codon designed in the phage-displayed library and their coverage of the natural diversity (degenerate codons: D = A/G/T; V = A/C/G; K = G/T; R = A/G; W = A/T; H = A/C/T).

mD9, we then designed a phage-displayed library under the structure-based conception, which has also been proven *in vivo* (Wu et al., 2015) to create hD9 variants only in the regions of HCDR3, LCDR1, and LCDR2 but not the essential LCDR3 to minimize the influence on the epitope-paratope interaction and structural integrity (Figure 5E). The design principle of phage-displayed library was adapted from Dr. Germaine Fuh's group (Sidhu et al., 2004), in which the diversity of the synthetic library

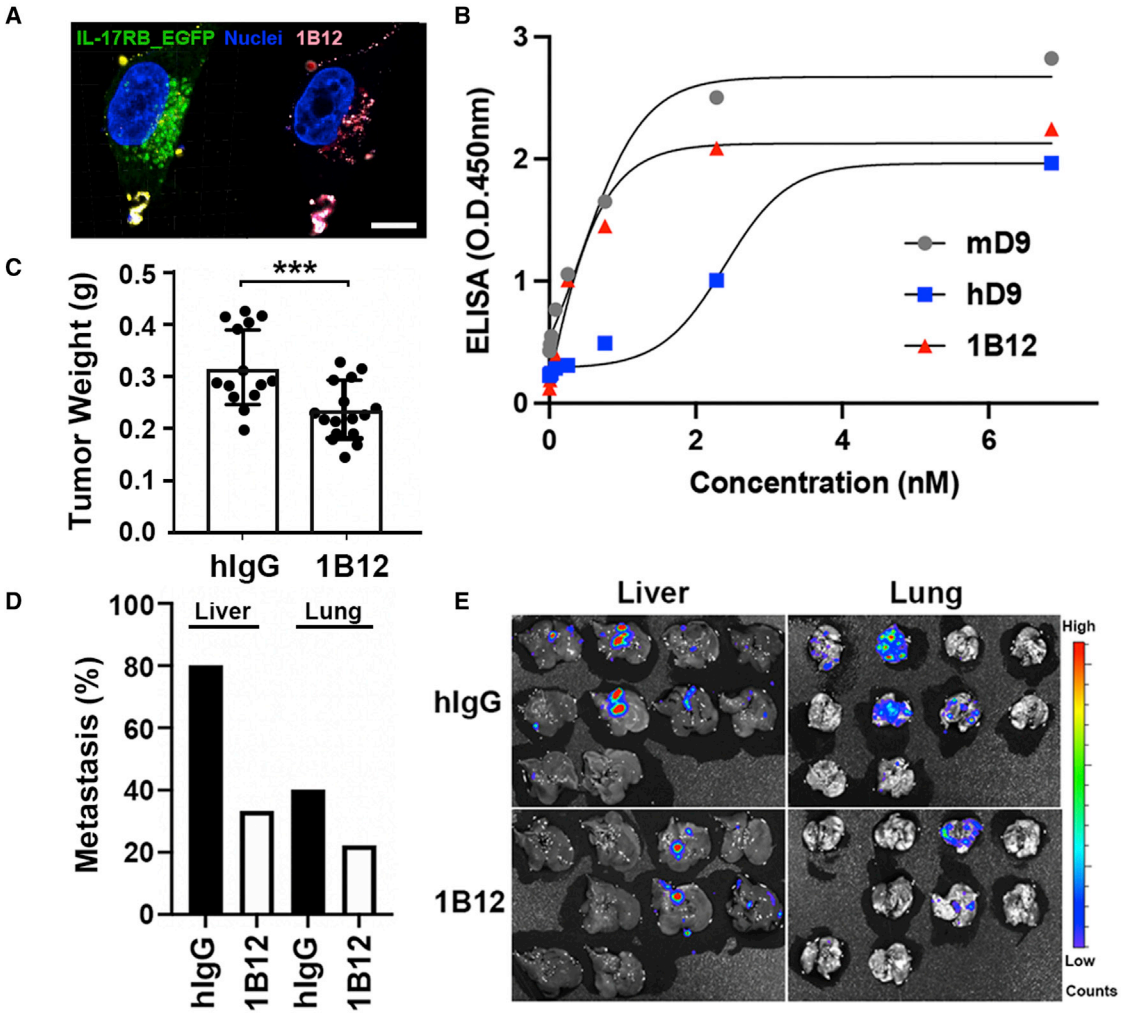

Figure 6. The binding specificity and neutralization potency of the affinity-matured humanized D9 antibody 1B12

(A) Confocal images of the HEK293T cells overexpressing IL-17RB-EGFP (green) showing the colocalization of 1B12 (pink) (scale bar, 10 μm).

(B) ELISA binding avidity of 1B12 compared with the parental clone hD9 and the original mouse mD9.

(C) Inhibition of tumor growth by 1B12 compared with the control IgG in a pancreatic orthotopic mouse model (n = 16 per group), showing as a significant lower tumor weight. Statistical analysis was performed using two-tailed paired Student's t tests ($p < 0.001$).

(D and E) From the metastasis studies, 1B12 exhibited better blocking activity against the metastasis of pancreatic tumors to lung and liver. The quantitative chart of the metastasis incidence between 1B12 and the control IgG group in (D).

is majorly designed from the natural prevalence of human antibody database to mimic the naïve gene repertoire (Figure 5F). We next calculated the occurring percentage of each amino acid at each site in HCDR3, LCDR1, and LCDR2 of the D9 paratope from the database of abYsis (www.abYsis.org), and designed the variants at residues of Y96, Y97, G98, and Y99 of HCDR3; S27, S29, I30, Y31, and Y32 of LCDR1; and Y48, D49, T50, S51, and K52 of LCDR2, with the tailored degenerate codons to cover the nature prevalence from 65% to 90% at each position as indicated (Figure 5G). Because the amino acid prevalence of HCDR3 is much more diverse than that of LCDR1 and LCDR2 (Figure 5E), we omitted the residues buried inside the structure, such as R98, S99, V104, D105, and Y106 of HCDR3. We then used the Kunkel method (Kunkel et al., 1987; Rouet et al., 2012) to randomize those residues on HCDR3, LCDR1, LCDR2, and three CDR combinations with the theoretical library size of 1.46×10^4, 6×10^2, 1.26×10^3, and 1.1×10^{10}, respectively (Figure 5E). These libraries were amplified with the hD9-scFv-variant carrying M13K07 phages and went through biopanning with Protein G dynabeads to immobilize the Fc-fused hIL-17RB and enrich the high-affinity scFv repertoire. Finally, an affinity-matured humanized antibody clone, 1B12, was selected for its high specificity and increased binding avidity to IL-17RB (half maximal effective concentration [EC50] of 0.535nM), which is five times higher than the parent clone mD9 (EC50 of 2.634nM) (Figures 6A and 6B).

This 1B12 antibody carries all four residues of LCDR1 mutated from S-S-I-Y to N-I-G-K, two residues of LCDR2 mutated as D49K and S52N, and residues of HCDR3 mutated from Y-Y-G-Y to D-N-S-R. These mutations probably contribute to around

2-fold affinity elevation comparing to the parental antibody hD9 in ELISA (Figure 6B). In the mouse orthotopic model, injections of 1B12 (5 mg/kg per week) can significantly decrease the tumor growth and metastasis compared with the control human IgG, as demonstrated by the tumor weight of the 1B12 group being 1.34× smaller than the control (Figures 6C–6E). These results suggest that the affinity maturation of hD9, such as the resulting humanized 1B12 antibody, can efficiently recognize hIL-17RB with similar affinity and inhibit the proliferation of pancreatic cancer cells *in vivo*.

DISCUSSION

The IL-17RB/IL-17B signaling plays an important role in modulating the immune defense system in a way distinct from its well-known homologue, IL-17RA. Beyond the immune response, the IL-17B/IL-17RB autocrine loop can induce proliferation, metastasis, and invasion of several types of tumors to promote disease progression and reduce the survival of cancer patients. Here, we have solved the structure of IL-17RB ectodomain, which contains the two similar FnIII-fold domains as IL-17RA, with different distributions of disulfide bridges and N-glycosylation sites. Based on this structure and other reported ones, we found the angle between two FnIII domains of IL-17 receptors may be smaller in the ligand-free state than the ligand-bound (Ely et al., 2009; Goepfert et al., 2017; Liu et al., 2013). Ligand binding could induce a conformational change of the two FnIII domains to open up a space that may facilitate the recruitment of the second receptor for receptor dimerization and downstream signaling transduction (Wu et al., 2021). Furthermore, we reported the complex structure of IL-17RB with its neutralizing antibody D9 Fab, highlighting the flexibility of the A′-A loop, which can be flipped and bended in a distinct conformation, and it awaits further investigation whether it is an induced fit as D9 antibody functions in the neutralizing niche.

The mouse monoclonal antibody D9 (mD9) has been reported as a therapeutic intervention in a pancreatic orthotopic model (Wu et al., 2021). However, mD9 is from the mouse origin and its humanization is a necessary process for future clinical applications, with otherwise undesired elicitation of anti-mouse human antibodies. Thus, we grafted six CDRs of mD9 to the framework of Trastuzumab to generate the humanized hD9 resulting in a marginal decrease of affinity compared with parental clone mD9. To rescue the affinity, we used the structural information and alanine-scanning results of the interacting CDR residues to guide the design of phage-display libraries of LCDR1, LCDR2, and HCDR3 for selecting IL-17RB-specific antibody clones with the highest affinity. The affinity-matured 1B12 antibody can not only bind to IL-17RB with higher affinity and specificity, but also decrease tumor growth and metastasis *in vivo*, potentially by blocking the IL-17B/IL-17RB signaling in a mouse tumor orthotopic experiment.

Although the humanized antibody 1B12 can block the signaling of IL-17RB/IL-17B, it is still unknown if its epitope is the same as that of the original mD9. There is another ligand IL-17E (IL-25) capable of binding to the receptor heterodimer of IL-17RB/IL-17RA (Lee et al., 2001; Rickel et al., 2008). Whether 1B12 antibody can affect the interaction between IL-17E and the heterodimeric IL-17A/B receptors remains to be elucidated. Moreover, it is unknown if IgG1 1B12 antibody would possibly induce ADCC/CDC allergic immune response. The other Fc, such as IgG4 or IgG1 silenced mutant P329G LALA, should be compared in a mouse model. In addition, the affinity maturation procedure has been limited to three CDRs that are adjacent to most important interacting loop LCDR3. There is still a possibility that the mutations on HCDR1 and HCDR2 can bring in additional binding strength of the humanized D9 to IL-17RB, which will altogether affect the effective inhibition of tumor growth by 1B12 in our mouse model.

In conclusion, with an urgent need of the pancreatic-cancer-specific treatment, IL-17RB-dependent signaling pathways have become attractive targets. In this work, we used the glycan-removed IL-17RB ECD as the immunogen to stimulate high immune response in mice and selected an IL-17RB neutralizing antibody D9 verified by flow cytometry and soft agar colony formation assay. We further solved the structure of the high homologous bIL-17RB ECD in complex with D9 Fab and proposed its neutralization mechanism. Based on the structural interface and alanine-scanning results, we designed the humanization and affinity maturation of antibody D9. The affinity-matured humanized antibody 1B12 was proven to inhibit pancreatic cancer growth in a mouse orthotopic model. Although it is still in the very preliminary stage for the development of the IL-17RB antagonist antibody, these results have undoubtedly become a key step forward and suggested the potential value of D9 and 1B12 in the therapeutic application for cancer treatments in the future.

STAR★METHODS

Detailed methods are provided in the online version of this paper and include the following:

- KEY RESOURCES TABLE
- RESOURCE AVAILABILITY
  - Lead contact
  - Materials availability
  - Data and code availability
- EXPERIMENTAL MODEL AND SUBJECT DETAILS
  - Cell lines
  - Animals
- METHOD DETAILS
  - Protein constructs
  - Protein expression and purification
  - Immunization and hybridoma fusion
  - Enzyme linked immunosorbent assay (ELISA)
  - Flow cytometry
  - Soft agar colony formation assay
  - Variable region cloning of mAb D9
  - Complementary determining regions grafting
  - Bio-layer interferometry (BLI)
  - Epitope mapping via phage display biopanning
  - Kunkel mutagenesis
  - Fab preparation
  - Alanine scanning of D9 antibody
  - Structure modeling
  - Crystallization
  - Structure determination and refinement

- Phage-display library design for affinity maturation
- Phage-display bio-panning for affinity maturation
- Immunofluorescence
- Pancreatic cancer orthotopic mouse experiment

- QUANTIFICATION AND STATISTICAL ANALYSIS

SUPPLEMENTAL INFORMATION

Supplemental information can be found online at https://doi.org/10.1016/j.celrep.2022.111555.

ACKNOWLEDGMENTS

We thank the staffs at beamline TPS, National Synchrotron Radiation Research Center (NSRRC), Taiwan, for their assistance with X-ray data collection. We also thank the Biophysical Core Facility, Academia Sinica, for providing technical advice for the biolayer interferometry experiment. We also thank Dr. T.W. Chang for providing the immunoglobulin expression vector. This work was supported by the Genomics Research Center Summit Project of Academia Sinica AS-SUMMIT-109 to C.M., AS-GC-110-MD03 and AS-KPQ-111-KNT to C.M.H.; the higher 10 education sprout project by the Ministry of Education, Taiwan via the "Drug Development Center of China Medical University" to W.HwaL.

AUTHOR CONTRIBUTIONS

C.M. and W.HwaL. conceived the idea. W.HsinL. designed and executed the study. W.HsinL. isolated, humanized, and affinity-matured the antibodies. W.HsinL. crystallized the protein complex and solved the structure. W.HsinL. and J.H.L. performed the mouse experiments. W.HsinL. and X.R.C. prepared the initial draft of this work. I.J.L. and H.C.W. performed phage-displayed random peptide library assay and provided the phage-displayed library techniques. X.R.C., W.HwaL., and C.M. reviewed and edited the manuscript. W.HwaL., C.M., C.M.H., and S.K.W. supervised this work.

DECLARATION OF INTERESTS

The authors declare no competing interests.

Received: February 21, 2022
Revised: August 22, 2022
Accepted: October 2, 2022
Published: October 25, 2022

REFERENCES

Adams, R., Maroof, A., Baker, T., Lawson, A.D.G., Oliver, R., Paveley, R., Rapecki, S., Shaw, S., Vajjah, P., West, S., and Griffiths, M. (2020). Bimekizumab, a novel humanized IgG1 antibody that neutralizes both IL-17A and IL-17F. Front. Immunol. *11*, 1894. https://doi.org/10.3389/fimmu.2020.01894.

Afonine, P.V., Grosse-Kunstleve, R.W., Echols, N., Headd, J.J., Moriarty, N.W., Mustyakimov, M., Terwilliger, T.C., Urzhumtsev, A., Zwart, P.H., and Adams, P.D. (2012). Towards automated crystallographic structure refinement with phenix.refine. Acta Crystallogr D Biol Crystallogr *68*, 352–367. https://doi.org/10.1107/S0907444912001308.

Armstrong, A.W., and Read, C. (2020). Pathophysiology, clinical presentation, and treatment of psoriasis: a review. JAMA *323*, 1945–1960. https://doi.org/10.1001/jama.2020.4006.

Barlow, J.L., and McKenzie, A.N.J. (2009). IL-25: a key requirement for the regulation of type-2 immunity. Biofactors *35*, 178–182. https://doi.org/10.1002/biof.24.

Bie, Q., Sun, C., Gong, A., Li, C., Su, Z., Zheng, D., Ji, X., Wu, Y., Guo, Q., Wang, S., and Xu, H. (2016). Non-tumor tissue derived interleukin-17B activates IL-17RB/AKT/beta-catenin pathway to enhance the stemness of gastric cancer. Sci. Rep. *6*, 25447. https://doi.org/10.1038/srep25447.

Brembilla, N.C., Senra, L., and Boehncke, W.H. (2018). The IL-17 family of cytokines in psoriasis: IL-17A and beyond. Front. Immunol. *9*, 1682. https://doi.org/10.3389/fimmu.2018.01682.

Brochet, X., Lefranc, M.P., and Giudicelli, V. (2008). IMGT/V-QUEST: the highly customized and integrated system for IG and TR standardized V-J and V-D-J sequence analysis. Nucleic Acids Res. *36*, W503–W508. https://doi.org/10.1093/nar/gkn316.

Chen, J.R., Yu, Y.H., Tseng, Y.C., Chiang, W.L., Chiang, M.F., Ko, Y.A., Chiu, Y.K., Ma, H.H., Wu, C.Y., Jan, J.T., et al. (2014). Vaccination of monoglycosylated hemagglutinin induces cross-strain protection against influenza virus infections. Proc. Natl. Acad. Sci. USA *111*, 2476–2481. https://doi.org/10.1073/pnas.1323954111.

Corpet, F. (1988). Multiple sequence alignment with hierarchical clustering. Nucleic Acids Res. *16*, 10881–10890. https://doi.org/10.1093/nar/16.22.10881.

Echols, N., Morshed, N., Afonine, P.V., McCoy, A.J., Miller, M.D., Read, R.J., Richardson, J.S., Terwilliger, T.C., and Adams, P.D. (2014). Automated identification of elemental ions in macromolecular crystal structures. Acta Crystallogr. D Biol. Crystallogr. *70*, 1104–1114. https://doi.org/10.1107/S1399004714001308.

Ely, L.K., Fischer, S., and Garcia, K.C. (2009). Structural basis of receptor sharing by interleukin 17 cytokines. Nat. Immunol. *10*, 1245–1251.

Emsley, P., and Cowtan, K. (2004). Coot: model-building tools for molecular graphics. Acta Crystallogr. D Biol. Crystallogr. *60*, 2126–2132. https://doi.org/10.1107/S0907444904019158.

Emsley, P., Lohkamp, B., Scott, W.G., and Cowtan, K. (2010). Features and development of Coot. Acta Crystallogr. D Biol. Crystallogr. *66*, 486–501. https://doi.org/10.1107/S0907444910007493.

Essono, S., Frobert, Y., Grassi, J., Créminon, C., and Boquet, D. (2003). A general method allowing the design of oligonucleotide primers to amplify the variable regions from immunoglobulin cDNA. J. Immunol. Methods *279*, 251–266. https://doi.org/10.1016/s0022-1759(03)00242-4.

Gaffen, S.L. (2009). Structure and signalling in the IL-17 receptor family. Nat. Rev. Immunol. *9*, 556–567.

Gelaleti, G.B., Borin, T.F., Maschio-Signorini, L.B., Moschetta, M.G., Jardim-Perassi, B.V., Calvinho, G.B., Facchini, M.C., Viloria-Petit, A.M., and de Campos Zuccari, D.A.P. (2017). Efficacy of melatonin, IL-25 and siIL-17B in tumorigenesis-associated properties of breast cancer cell lines. Life Sci. *183*, 98–109. https://doi.org/10.1016/j.lfs.2017.06.013.

Goddard, T.D., Huang, C.C., Meng, E.C., Pettersen, E.F., Couch, G.S., Morris, J.H., and Ferrin, T.E. (2018). UCSF ChimeraX: meeting modern challenges in visualization and analysis. Protein Sci. *27*, 14–25. https://doi.org/10.1002/pro.3235.

Goepfert, A., Lehmann, S., Wirth, E., and Rondeau, J.M. (2017). The human IL-17A/F heterodimer: a two-faced cytokine with unique receptor recognition properties. Sci. Rep. *7*, 8906. https://doi.org/10.1038/s41598-017-08360-9.

Harrington, L.E., Hatton, R.D., Mangan, P.R., Turner, H., Murphy, T.L., Murphy, K.M., and Weaver, C.T. (2005). Interleukin 17-producing CD4+ effector T cells develop via a lineage distinct from the T helper type 1 and 2 lineages. Nat. Immunol. *6*, 1123–1132. https://doi.org/10.1038/ni1254.

He, H., Fang, H., Miller, M.D., Phillips, G.N., Jr., and Su, W.P. (2016). Improving the efficiency of molecular replacement by utilizing a new iterative transform phasing algorithm. Acta Crystallogr. A Found. Adv. *72*, 539–547. https://doi.org/10.1107/S2053273316010731.

Huang, C.K., Yang, C.Y., Jeng, Y.M., Chen, C.L., Wu, H.H., Chang, Y.C., Ma, C., Kuo, W.H., Chang, K.J., Shew, J.Y., and Lee, W.H. (2014). Autocrine/paracrine mechanism of interleukin-17B receptor promotes breast tumorigenesis through NF-kappaB-mediated antiapoptotic pathway. Oncogene *33*, 2968–2977. https://doi.org/10.1038/onc.2013.268.

Huang, H.Y., Liao, H.Y., Chen, X., Wang, S.W., Cheng, C.W., Shahed-Al-Mahmud, M., Liu, Y.M., Mohapatra, A., Chen, T.H., Lo, J.M., et al. (2022). Vaccination with SARS-CoV-2 spike protein lacking glycan shields elicits enhanced protective responses in animal models. Sci. Transl. Med. *14*, eabm0899. https://doi.org/10.1126/scitranslmed.abm0899.

Huang, S.C., Wei, P.C., Hwang-Verslues, W.W., Kuo, W.H., Jeng, Y.M., Hu, C.M., Shew, J.Y., Huang, C.S., Chang, K.J., Lee, E.Y.H., and Lee, W.H.

(2017). TGF-beta1 secreted by Tregs in lymph nodes promotes breast cancer malignancy via up-regulation of IL-17RB. EMBO Mol. Med. *9*, 1660–1680. https://doi.org/10.15252/emmm.201606914.

Krebber, A., Bornhauser, S., Burmester, J., Honegger, A., Willuda, J., Bosshard, H.R., and Plückthun, A. (1997). Reliable cloning of functional antibody variable domains from hybridomas and spleen cell repertoires employing a reengineered phage display system. J. Immunol. Methods *201*, 35–55. https://doi.org/10.1016/s0022-1759(96)00208-6.

Kunkel, T.A., Roberts, J.D., and Zakour, R.A. (1987). Rapid and efficient site-specific mutagenesis without phenotypic selection. Methods Enzymol. *154*, 367–382.

Laprevotte, E., Cochaud, S., du Manoir, S., Lapierre, M., Dejou, C., Philippe, M., Giustiniani, J., Frewer, K.A., Sanders, A.J., Jiang, W.G., et al. (2017). The IL-17B-IL-17 receptor B pathway promotes resistance to paclitaxel in breast tumors through activation of the ERK1/2 pathway. Oncotarget *8*, 113360–113372. https://doi.org/10.18632/oncotarget.23008.

Lee, J., Ho, W.H., Maruoka, M., Corpuz, R.T., Baldwin, D.T., Foster, J.S., Goddard, A.D., Yansura, D.G., Vandlen, R.L., Wood, W.I., and Gurney, A.L. (2001). IL-17E, a novel proinflammatory ligand for the IL-17 receptor homolog IL-17Rh1. J. Biol. Chem. *276*, 1660–1664.

Lefranc, M.P., Giudicelli, V., Ginestoux, C., Jabado-Michaloud, J., Folch, G., Bellahcene, F., Wu, Y., Gemrot, E., Brochet, X., Lane, J., Regnier, L., Ehrenmann, F., Lefranc, G., and Duroux, P. (2009). IMGT, the international ImMunoGeneTics information system. Nucleic Acids Res. *37*, Epub 2008 Oct 31. https://doi.org/10.1093/nar/gkn838.

Liebschner, D., Afonine, P.V., Baker, M.L., Bunkóczi, G., Chen, V.B., Croll, T.I., Hintze, B., Hung, L.W., Jain, S., McCoy, A.J., et al. (2019). Macromolecular structure determination using X-rays, neutrons and electrons: recent developments in Phenix. Acta Crystallogr. D Struct. Biol. *75*, 861–877. https://doi.org/10.1107/S2059798319011471.

Liu, S. (2019). Structural insights into the interleukin-17 family cytokines and their receptors. Adv. Exp. Med. Biol. *1172*, 97–117. https://doi.org/10.1007/978-981-13-9367-9_5.

Liu, S., Desharnais, J., Sahasrabudhe, P.V., Jin, P., Li, W., Oates, B.D., Shanker, S., Banker, M.E., Chrunyk, B.A., Song, X., et al. (2016). Inhibiting complex IL-17A and IL-17RA interactions with a linear peptide. Sci. Rep. *6*, 26071. https://doi.org/10.1038/srep26071.

Liu, S., Song, X., Chrunyk, B.A., Shanker, S., Hoth, L.R., Marr, E.S., and Griffor, M.C. (2013). Crystal structures of interleukin 17A and its complex with IL-17 receptor A. Nat. Commun. *4*, 1888. https://doi.org/10.1038/ncomms2880.

Maitra, A., Shen, F., Hanel, W., Mossman, K., Tocker, J., Swart, D., and Gaffen, S.L. (2007). Distinct functional motifs within the IL-17 receptor regulate signal transduction and target gene expression. Proc. Natl. Acad. Sci. USA *104*, 7506–7511. https://doi.org/10.1073/pnas.0611589104.

McGeachy, M.J., Cua, D.J., and Gaffen, S.L. (2019). The IL-17 family of cytokines in health and disease. Immunity *50*, 892–906. https://doi.org/10.1016/j.immuni.2019.03.021.

Papp, K.A., Leonardi, C., Menter, A., Ortonne, J.P., Krueger, J.G., Kricorian, G., Aras, G., Li, J., Russell, C.B., Thompson, E.H.Z., and Baumgartner, S. (2012). Brodalumab, an anti-interleukin-17-receptor antibody for psoriasis. N. Engl. J. Med. *366*, 1181–1189. https://doi.org/10.1056/NEJMoa1109017.

Park, H., Li, Z., Yang, X.O., Chang, S.H., Nurieva, R., Wang, Y.H., Wang, Y., Hood, L., Zhu, Z., Tian, Q., and Dong, C. (2005). A distinct lineage of CD4 T cells regulates tissue inflammation by producing interleukin 17. Nat. Immunol. *6*, 1133–1141. https://doi.org/10.1038/ni1261.

Pettersen, E.F., Goddard, T.D., Huang, C.C., Meng, E.C., Couch, G.S., Croll, T.I., Morris, J.H., and Ferrin, T.E. (2021). UCSF ChimeraX: structure visualization for researchers, educators, and developers. Protein Sci. *30*, 70–82. https://doi.org/10.1002/pro.3943.

Powell, H.R., Johnson, O., and Leslie, A.G.W. (2013). Autoindexing diffraction images with iMosflm. Acta Crystallogr. D Biol. Crystallogr. *69*, 1195–1203. https://doi.org/10.1107/S0907444912048524.

Reeves, P.J., Callewaert, N., Contreras, R., and Khorana, H.G. (2002). Structure and function in rhodopsin: high-level expression of rhodopsin with restricted and homogeneous N-glycosylation by a tetracycline-inducible N-acetylglucosaminyltransferase I-negative HEK293S stable mammalian cell line. Proc. Natl. Acad. Sci. USA *99*, 13419–13424. https://doi.org/10.1073/pnas.212519299.

Rickel, E.A., Siegel, L.A., Yoon, B.R.P., Rottman, J.B., Kugler, D.G., Swart, D.A., Anders, P.M., Tocker, J.E., Comeau, M.R., and Budelsky, A.L. (2008). Identification of functional roles for both IL-17RB and IL-17RA in mediating IL-25-induced activities. J. Immunol. *181*, 4299–4310. https://doi.org/10.4049/jimmunol.181.6.4299.

Rouet, R., Dudgeon, K., and Christ, D. (2012). Generation of human single domain antibody repertoires by Kunkel mutagenesis. Methods Mol. Biol. *907*, 195–209. https://doi.org/10.1007/978-1-61779-974-7_10.

Sidhu, S.S., Li, B., Chen, Y., Fellouse, F.A., Eigenbrot, C., and Fuh, G. (2004). Phage-displayed antibody libraries of synthetic heavy chain complementarity determining regions. J. Mol. Biol. *338*, 299–310. https://doi.org/10.1016/j.jmb.2004.02.050.

Swaidani, S., Bulek, K., Kang, Z., Liu, C., Lu, Y., Yin, W., Aronica, M., and Li, X. (2009). The critical role of epithelial-derived Act1 in IL-17- and IL-25-mediated pulmonary inflammation. J. Immunol. *182*, 1631–1640. https://doi.org/10.4049/jimmunol.182.3.1631.

Swindells, M.B., Porter, C.T., Couch, M., Hurst, J., Abhinandan, K.R., Nielsen, J.H., Macindoe, G., Hetherington, J., and Martin, A.C.R. (2017). abYsis: integrated antibody sequence and structure-management, analysis, and prediction. J. Mol. Biol. *429*, 356–364. https://doi.org/10.1016/j.jmb.2016.08.019.

UniProt Consortium (2021). UniProt: the universal protein knowledgebase in 2021. Nucleic Acids Res. *49*, D480–D489. https://doi.org/10.1093/nar/gkaa1100.

Vitiello, G.A., and Miller, G. (2020). Targeting the interleukin-17 immune axis for cancer immunotherapy. J. Exp. Med. *217*, e20190456. https://doi.org/10.1084/jem.20190456.

Waterhouse, A., Bertoni, M., Bienert, S., Studer, G., Tauriello, G., Gumienny, R., Heer, F.T., de Beer, T.A.P., Rempfer, C., Bordoli, L., et al. (2018). SWISS-MODEL: homology modelling of protein structures and complexes. Nucleic Acids Res. *46*, W296–W303. https://doi.org/10.1093/nar/gky427.

Wilson, S.C., Caveney, N.A., Yen, M., Pollmann, C., Xiang, X., Jude, K.M., Hafer, M., Tsutsumi, N., Piehler, J., and Garcia, K.C. (2022). Organizing structural principles of the interleukin-17 ligand-receptor Axis. Nature *609*, 622–629. https://doi.org/10.1038/s41586-022-05116-y.

Wu, H.H., Hwang-Verslues, W.W., Lee, W.H., Huang, C.K., Wei, P.C., Chen, C.L., Shew, J.Y., Lee, E.Y.H.P., Jeng, Y.M., Tien, Y.W., et al. (2015). Targeting IL-17B-IL-17RB signaling with an anti-IL-17RB antibody blocks pancreatic cancer metastasis by silencing multiple chemokines. J. Exp. Med. *212*, 333–349. https://doi.org/10.1084/jem.20141702.

Wu, H.H., Tsai, L.H., Huang, C.K., Hsu, P.H., Chen, M.Y., Chen, Y.I., Hu, C.M., Shen, C.N., Lee, C.C., Chang, M.C., et al. (2021). Characterization of initial key steps of IL-17 receptor B oncogenic signaling for targeted therapy of pancreatic cancer. Sci. Transl. Med. *13*, eabc2823. https://doi.org/10.1126/scitranslmed.abc2823.

Yang, Y.F., Lee, Y.C., Lo, S., Chung, Y.N., Hsieh, Y.C., Chiu, W.C., and Yuan, S.S.F. (2018). A positive feedback loop of IL-17B-IL-17RB activates ERK/beta-catenin to promote lung cancer metastasis. Cancer Lett. *422*, 44–55. https://doi.org/10.1016/j.canlet.2018.02.037.

Zwart, P.H., Afonine, P.V., Grosse-Kunstleve, R.W., Hung, L.W., Ioerger, T.R., McCoy, A.J., McKee, E., Moriarty, N.W., Read, R.J., Sacchettini, J.C., et al. (2008). Automated structure solution with the PHENIX suite. Methods Mol. Biol. *426*, 419–435. https://doi.org/10.1007/978-1-60327-058-8_28.

Zwicky, P., Unger, S., and Becher, B. (2020). Targeting interleukin-17 in chronic inflammatory disease: a clinical perspective. J. Exp. Med. *217*, e20191123. https://doi.org/10.1084/jem.20191123.

CellPress
OPEN ACCESS

STAR★METHODS

KEY RESOURCES TABLE

REAGENT or RESOURCE	SOURCE	IDENTIFIER
Antibodies		
mD9	This paper	N/A
cD9	This paper	N/A
hD9	This paper	N/A
1B12	This paper	N/A
goat anti-mouse HRP	GeneTex	Cat# GTX77230; RRID: AB_378672
anti-M13 mAb	GE Healthcare Biosciences	Cat# NA931; RRID: AB_772210
Mouse Gamma Globulin	Jackson ImmunoResearch	Cat# 015-000-002; RRID: AB_2337187
Human Gamma Globulin	Jackson ImmunoResearch	Cat# 009-000-002; RRID: AB_2337042
Bacterial and virus strains		
M13K07 helper phage	New England BioLabs	N0315S
Phage-displayed 12-mer peptide library	New England BioLabs	E8111L
E. *coli* K12 ER2738	New England BioLabs	E4104
E. *coli* K12 CJ236	New England BioLabs	E4141
Biological samples		
FreeStyle™ 293 Expression Medium	Thermo Fisher Scientific	12338
WAVE Cellbag	Cytiva	CB0200L10-11
Fetal Bovine Serum (FBS)	Merck	TMS-013-BKR
Chemicals, peptides, and recombinant proteins		
Human IL-17RB (R18-P292)	This study	N/A
Bovine IL-17RB (E19 to G272)	This study	N/A
Polyethyleneimine MW 25000 (PEI 25K™)	Polyscience	23966–1
AcTEV™ Protease	Thermo Fisher Scientific	12575
Endoglycosidase H	New England BioLabs	P0702
Tetramethylbenzidine (TMB)	Thermo Fisher Scientific	34029
TRIzol	Thermo Fisher Scientific	15596
KOD Hot Start DNA Polymerase	Merck	71086
T4 polynucleotide kinase	New England BioLabs	M0201
L-Cysteine	Sigma-Aldrich	168149
Protein G Magnetic Beads	Thermo Fisher Scientific	88848
Pierce™ Protein A Agarose	Thermo Fisher Scientific	20333
Bicine	Molecular Dimensions	MD2-003-PH
PEG3350	Molecular Dimensions	MD2-100-9
Critical commercial assays		
Transcriptor One-Step RT-PCR Kit	Roche	4655877001
ExpiFectamine™ 293 Transfection Kit	Thermo Fisher Scientific	A14524
Deposited data		
Crystal Structure of bovine IL-17RB ECD with D9 Fab complex	PDB	7WG3
Experimental models: Cell lines		
HEK293 EBNA	American Type Culture Collection (ATCC)	CRL-10852
HEK293S GnTI$^-$	American Type Culture Collection (ATCC)	CRL-3022
HEK293T	American Type Culture Collection (ATCC)	CRL-3126
TG1 Electrocompetent Cells	Lucigen	60502
CFPAC-1	American Type Culture Collection (ATCC)	CRL-1918

(*Continued on next page*)

Continued

REAGENT or RESOURCE	SOURCE	IDENTIFIER
Expi293F	Thermo Fisher Scientific	A14527
Experimental models: Organisms/strains		
BALB/c	National Laboratory Animal Center, Taiwan	N/A
NOD.Cg-*Prkdc*^{scid} *Il2rg*^{tm1Wjl}/SzJ (NSG) mice	The Jackson Laboratory	#005557
Oligonucleotides		
Codon optimized human IL-17RB sequence	Eurofins MWG Operon	2436448/Liu
Codon optimized bovine IL-17RB sequence	Eurofins MWG Operon	2436448/Liu
Recombinant DNA		
Codon optimized human IL-17RB sequence	Eurofins MWG Operon	2436448/Liu
Codon optimized bovine IL-17RB sequence	Eurofins MWG Operon	2436448/Liu
Plasmid pTT-GS-strep-8His	This paper	N/A
Plasmid pcDNA3.1	Thermo Fisher Scientific	V79020
Plasmid pCR^{TM}2.1	Thermo Fisher Scientific	K200001
Plasmid pCANTAB5E	Pharmacia	N/A
Software and algorithms		
IMGT®, the international ImMunoGeneTics information system	Lefranc et al., 2009	N/A
Multalin	Corpet (1988)	N/A
SWISS-MODEL	Waterhouse et al. (2018)	N/A
iMosflm	Powell et al. (2013)	N/A
Phenix.phaser-MR	Liebschner et al. (2019)	N/A
Phenix.refine	Liebschner et al. (2019)	N/A
Coot	Emsley and Cowtan (2004)	N/A
PyMol	Schrödinger	N/A
UCSF Chimera X	Pettersen et al. (2021)	N/A
abYsis	Swindells et al. (2017)	N/A
GraphPad Prism 7	Graphpad	N/A
Other		
Octet® Anti-Human Fc Capture (AHC) Biosensors	Sartorius	18–5060

RESOURCE AVAILABILITY

Lead contact

Further information and requests for resources and reagents should be directed to the lead contact, Che Ma (cma@gate.sinica.edu.tw).

Materials availability

The unique/stable reagents generated in this study are available from the lead contact with a completed Materials Transfer Agreement.

Data and code availability

The coordinates and structure factors have been deposited at Protein Data Bank (ID: 7WG3) and are publicly available as of the date of publication. This paper does not report original code. Any additional information required to reanalyze the data reported in this paper is available from the lead contact upon request.

EXPERIMENTAL MODEL AND SUBJECT DETAILS

Cell lines

N-acetylglucosaminyltransferase I deficient (GnTI^{-}) HEK293S cells, HEK293 EBNA cells, HEK293T, CFPAC-1 cells were bought from American Type Culture Collection, ATCC. Expi293F cells were bought from Thermo Fisher Scientific. TG1 cells were bought from Lucigen.

Animals

8-week-old female BALB/c mice were obtained from National Laboratory Animal Center, Taipei, Taiwan. 10-week-old NOD/SCIDγ mice were obtained from animal core facility of Genomic Research Center, Academia Sinica.

METHOD DETAILS

Protein constructs

For immunostaining and flow cytometry assays, cDNA encoding the full-length human or bovine Interleukin-17B receptor (IL-17RB) was codon optimized (GenScript) with N-terminal fusion with the enhanced green fluorescent protein (EGFP) gene and constructed into the mammalian expression pTT vector. For protein expression and crystallization, the extracellular domain (ECD) of human or bovine IL-17RB (human sequence from R18 to P292; bovine sequence from E19 to G272) was cloned into pTT vector with a TEV cleavage site, a glycine-serine (GS) repeat linker, a strep-tag and a His_8 tag in tandem at the C terminus. The signal peptide M1-P17 of IL-17RB was replaced by ^{1}MGAARSPPSAVPGPLLGLLLLLLGVLAPGGAS^{32} from IL-17RA. The human IL17RB ECD (R18 to P292) was also cloned into pcDNA3.1 with C-terminal fusion with the Fc domain of human IgG1 for phage-display biopanning.

Protein expression and purification

The pTT-IL-17RB-GS-strep-His_8 plasmid was transiently transfected into the HEK293S cells and HEK293 EBNA cells by polyethyleneimine (PEI), and both cells were cultured in Freestyle 293 expression medium (Gibco) in wave bag system (Cytiva) at 37°C with 0.8% CO_2. The supernatant was harvested at day four by 6000 rpm centrifugation for 15 min and loaded onto the Ni-NTA affinity resin that was pre-equilibrated in 50mM Tris pH 8.0, 150mM NaCl, 30mM imidazole. The his-tagged IL-17RB protein was eluted by 50mM Tris pH 8.0, 150mM NaCl, 300mM imidazole and exchanged into an imidazole-free buffer through centrifugal filter (Amicon® Ultra, Millipore) with a molecular mass cutoff of 30KDa at 4000rpm. The purified protein was loaded onto gel filtration column Superdex 200 increase 10/300 GL (Cytiva) and then the peak fractions were pooled and concentrated down to 10 mg/mL. The protein was further digested with acTEV (Invitrogen) and Endoglycosidase H (Endo H, New England BioLabs) following the manufacturer's recommendation for releasing the tags and removing the glycan shield (mono-GlcNAc decorated IL-17RB). For crystallization of the bovine IL-17RB ECD protein, the concentration was 15 mg/mL. For immunization, ELISA, and phage-display biopanning, the mono-GlcNAc decorated, fully-glycosylated and the EGFP-fused human IL-17RB ECD proteins were stored at the concentration of 1 mg/mL.

Immunization and hybridoma fusion

BALB/c female mice at 8 weeks old (National Laboratory Animal Center) were immunized one i.p. with 40μg MG or FG hIL-17RB ECD in 50mM Tris pH8.0, 300mM NaCl at day 0 and two times i.M. with protein mix with 50μg Al(OH)3 adjuvant in total volume of 100μL (six mice in each group). Bleed mouse two days before each immunization for serum collection tested for ELISA titer. Four of the mice were boosted i.v. with 40μg hIL-17RB ECD MG in 50μL buffer at day 38 and sacrificed at day 47 to perform fusion. Mouse spleen cells were washed with 1xPBS and suspended in 20mL DMEM w/o serum. The mouse spleen cells were mixed with 4×10^{7} myeloma cells in health phase and pellet down at 900rpm for 5 min. The medium was removed, and the cell pellet was gently dispersed by finger tapping. The cells were dropped with 1mL PEG1500 in 37°C water bath by gently stirring within 2 min and were dropped with 9 mL DMEM for another 3 min. The fused cells were pellet down at 900rpm for 5 min and gently suspended in 40 mL complete DMEM w/w 10% BM condimed H1 Hybridoma cloning supplement (Roche) and 10% fetal calf serum. The cells were distributed for 50μL/well in 96 well plates and supplied with 50 μL/well complete DMEM w/w 1× HAT (Invitrogen) every two days. At day 9 or 10, 80μL/well medium was carefully removed and 100μL/well complete DMEM w/w 1× HAT every three days. The medium was tested ELISA at day 15 with hIL17RB ECD FG protein. The hybridoma cells in positive wells were limiting-diluted to obtained the monoclonals.

Enzyme linked immunosorbent assay (ELISA)

In the hybridoma screening, 100ng/well of FG hIL-17RB ECD was coated on 96 well polystyrene microplates (Corning) at 4°C overnight followed by 300μL/well 1xPBST (0.05% Tween-20) washing once. Then, 200μL/well of 10% skim milk in 1xPBS was added for blocking at 37°C for one hour. 100μL/well of the supernatant of the hybridoma cell culture was added and incubated at 37°C for 2 h and 50μL/well goat anti-mouse HRP (GeneTex, 1:5000 dilution) in 1× PBS was added as the secondary antibody. Three times of washing with 300μL/well 1xPBST was applied between each step. The absorbance result was read at 450nm by Multiskan™ GO Microplate Spectrophotometer (Thermo Fisher Scientific) after adding 100μL/well tetramethylbenzidine (TMB, Thermo Fisher Scientific) and stopped by 100μL/well H_2SO_4.

Flow cytometry

For the screening of hybridoma cells, HEK293 EBNA cells were transfected with the EGFP-fused full length hIL-17RB, incubated for three days at 37°C. 1×10^{6} cells were washed with 1 mL 1xPBS for two times at 200g centrifugal force. 200μL supernatant of the hybridoma culture was added into the washed HEK293 EBNA cells and incubated at 4°C for 1 h. After three times of 1mL 1xPBS washes, 200ul Cy5 anti-mouse antibody was added at 1:200 dilution in 1xPBS containing 0.5% Fetal Bovine Serum (FBS, Merck) and incubated at 4°C for 1 h. Before flow cytometry analysis, the cells were washed with 1% FBS in 1× PBS for three times and then analyzed on the FACS Canto II (BD Biosciences).

Soft agar colony formation assay

2,500 cells were cultured in the complete growth medium mixed with 0.35% agar over a layer of complete growth medium with 0.5% agar in 12-well plates. 50μL of serum-free medium containing 1μg D9 antibody purified from hybridoma supernatant, or a control mouse gamma globulin (Jackson ImmunoResearch) was added every week. On day 14, cells were stained with crystal violet and the stained colonies were counted.

Variable region cloning of mAb D9

The mRNA of the D9-secreting hybridoma cells was isolated by TRIzol (Thermo Fisher Scientific) and was reverse-transcribed into cDNA using Reverse transcription polymerase chain reaction (RT-PCR) (Transcriptor One-Step RT-PCR, Roche) as the template for variable regions. The variable regions of light chain and heavy chain were amplified by primer sets from works of S. Essono and Krebber A. (Essono et al., 2003; Krebber et al., 1997). The reverse primer sets of each chain contain five primers located in the constant regions of the light and heavy chains. The forward primer sets of the heavy chain include three sets of MHV78, MHV9, and MHV12 and those of the light chain include another three sets of MKV75, MKV12A, and MKV12B. The reaction was mixed with 2μL of 10μM forward and reverse primer sets, 100ng cDNA template from D9 hybridoma cells, 1U of Taq DNA polymerase (KOD Hot Start DNA Polymerase, Merck), pre-mixed reaction buffer, and ddH_2O in a final volume of 25μL. The polymerase chain reaction (PCR) was hot started at 94°C followed by 30 cycles of 30s at 94°C, 30s at 55°C, 30s at 72°C and 2 min at 72°C. The result was analyzed by agarose gel electrophoresis and the DNA fragments around 400bps were sliced for gel extraction. The purified DNA fragments were then cloned into pCR2.1 (Thermo Fisher Scientific) by TA cloning method. The single colonies were inoculated into 2mL LB broth with 50μg/mL ampicillin cultured at 37°C overnight for mini-prep (Thermo Fisher Scientific). The light chain and heavy chain of D9 were cloned into a human immunoglobulin G1 vector (IgG vector; a gift from Dr. Tse-Wen Chang) and recombinantly expressed in Expi293F cells (Gibco) to be a mouse-variable human-constant chimeric antibody.

Complementary determining regions grafting

The variable region sequences of mouse D9 antibody was defined as six complementary determining regions (CDRs) by IMGT V-quest server (Brochet et al., 2008) of *Mus musculus* and was sequence-aligned following by Kabat numbering scheme. The CDRs of heavy chain were defined as HCDR1 from G26 to T33, HCDR2 from N52 to T57, and HCDR3 from R94 to Y102; the CDR regions of the light chain were LCDR1 from S27 to Y32, LCDR2 from Y49 to K53, and LCDR3 from Q89 to T97. The heavy chain and light chains were then aligned with human antibody germline sequences by IMGT V-quest of *homo sapiens*. The most similar human heavy chain to mouse D9 heavy chain was IGHV1-2*02F and most similar light chain is IGKV7-3*01P. The fragments of CDRs defined by IMGT V-quest server of *Mus musculus* were grafted into the framework of Trastuzumab.

Bio-layer interferometry (BLI)

Anti-Human IgG Fc Capture (AHC) biosensors was loaded with 10μM hIL-17RB ECD conjugated with Fc in 200μL 1xPBS for 300 s and the baseline was re-equilibrated in an equal volume of 1xPBS. The receptor bound AHC sensor was then dipped into the serially diluted mD9 or hD9 samples from concentration of 500nM to 0.06nM for 900 s. The dissociation was performed in the same buffer as baseline for 900 s. The data were collected by Octet Red96 and analyzed by Data Analysis 7.0 evaluation software.

Epitope mapping via phage display biopanning

The 8-well module was coated with mD9 at the concentration of 50 μg/mL in coating buffer (0.1 M $NaHCO_3$) and blocked with blocking buffer (1% BSA in PBS) at 4°C overnight. The phage-displayed random peptide library (4×10^{10} phages) (New England BioLabs) was incubated with the mD9-coated wells for 50 min at RT. After washing with $PBST_{0.5}$ (0.5% Tween 20 in PBS) six times, the bound phages were eluted with elution buffer (0.2 M Glycine, pH 2.2) and neutralized with 1 M Tris-HCl, pH 9.1. The eluted phages were cultured with E.*coli* K12 ER2738 (New England Biolabs) overnight culture by vigorously shaking for 4.5 h at 37°C. After centrifugation at 8,000 × g at 4°C, amplified phages in the supernatant were precipitated with 20% polyethylene glycol-8000 in 2.5 M NaCl (PEG/NaCl) at 4°C overnight. Then, precipitated phages were centrifuged for 20 min at 12,000 × g at 4°C and resuspended with PBS. The phages were re-precipitated with PEG/NaCl for 40 min at 4°C, isolated by centrifugation at 4°C for 10 min and re-suspended in 200 μL 1% BSA. The purified phages were tittered on LB/IPTG/X-Gal plates. The second to fourth rounds were identical to the first one except for the addition of 2×10^{11} plaque forming units (pfu) from previously amplified phages. The third or fourth round eluted phages were tittered on LB/IPTG/X-Gal plates and selected for ELISA. The ELISA plate was coated with 1 μg/mL of mD9, hD9, or control mouse gamma globulin (Jackson ImmunoResearch) in coating buffer for 2 h at RT and blocked with blocking buffer at 4°C overnight. The selected phages from LB/IPTG/X-Gal plates were incubated with coated plates for 1 h at RT. After washing with 0.5% PBST, the bound phages were detected with HRP-conjugated mouse anti-M13 mAb (1: 5,000 dilution) (GE Healthcare Biosciences). Then, the washed plates were incubated with TMB (Sigma-Aldrich, St. Louis, MO), and the reaction was stopped with 2 N H_2SO_4, with the plates being read using a microplate reader at 450 nm. The immunopositive phage clones were further sequenced with the −96 primer 5′-CCCTCATAGTTAGCGTAACG-3′, which corresponded to the pIII gene sequence of M13 phage. The phage-displayed peptide sequences were analyzed and aligned with Multalin tool (Corpet, 1988). ELISA plates were coated with mD9 or control mouse gamma globulin (Jackson ImmunoResearch) at a concentration of 1 μg/mL and blocked with blocking buffer at 4°C overnight. The plates were incubated with individual phages in three-fold serial dilution and the control

(helper phage). After washing with $PBST_{0.5}$, the plate was incubated with HRP-conjugated anti-M13 mAb for 1 h at RT, followed by the same procedures described above under "ELISA."

Kunkel mutagenesis

The *E.coli* strain CJ236 (New England BioLabs) was used for producing uracilated single-stranded DNA of as the cloning template. The dUTPase and N-glycosylase play important roles in the DNA repairing of *E. coli* cells and the replication of DNA by removing uracil from genome incorporation. The phagemid pCANTAB-5E (GE Healthcare) was chemically transformed into CJ236 on Luria-Bertani (LB) Broth plates w/w 17 μg/mL chloramphenicol, 20 μg/mL ampicillin and a single colony was inoculated to generate 50mL overnight culture with adding 5 × 10^8 cfu/μL M13K07 helper phage. The supernatant of the overnight culture was collected at 8000rpm centrifugation (rotor JLA16.25) and the phage particles were precipitated with polyethylene glycol (PEG)-NaCl on ice for 4 h, following a centrifugation at 12000rpm (rotor JLA16.25). The white pellet of phage particles on the tube bottom was resuspended in 1mL 100mM NaCl, 10mM Tris, pH8.0, 1mM EDTA in 2.0mL Eppendorf tubes. The suspension was added with 1mL buffer-saturated phenol, pH8.0 and was vortexed for 1 min, followed by 20rpm rotator-mixer for 15 min. Centrifugation at 14000 rpm for 15 min was applied for separating the phases. The upper layer was taken out carefully with 1mL chloroform added, vortexed for 1min, and then rocked at 20rpm for 15 min. Another centrifugation at 14000 rpm was applied for 15 min and then 300μL of 3M sodium acetate, 2mL 99% ethanol was added and mixed well. The sample was incubated on ice for 20minutes and centrifuged at 12000rpm for 20minutes. A small white-out pellet containing dU-single-stranded DNA template was dissolved in 30μL of 10mM Tri-HCl, pH7.6 and then was checked on 1% agarose gel. The mutagenic oligomers containing CDRH3/L1/L2 mutations were ordered from GenScript, Inc and were 5-terminal phosphrylated with T4 polynucleotide kinase (New England BioLabs). The Kunkel annealing reaction was performed in 50μL of 50mM Tris, 10mM $MgCl_2$, pH7.5 buffer with 1.5μL of each mutagenic oligomer, 4μg of dU-ssDNA template, and heated to 90°C then slowly cooling down to 20°C (1°C/min) (BioRad Mycycler). After annealing, the reaction was added with 5μL 10mM dNTP, 2μL 10mM ATP, 3μL 100mM DTT, 0.8μL T4 ligase, and 0.8μL T7 DNA polymerase at 20°C overnight for extension and ligation. The double-strand DNA products by Kunkel method were cleaned up by adding 400ul ddH_2O at 100g centrifugation in a 0.5mL Amicon MWCO 30K filter device for three times. The dsDNA was concentrated into around 30μL for electroporation.

Fab preparation

To prepare the Fab for crystallization, 10mg cD9 antibody was desalted in 20mM sodium phosphate, pH 7.0 through HiPrep 26/10 desalting column on AKTAxpress (GE Healthcare) and then concentrated into 10mg/mL. 10mM EDTA was added to the antibody. The antibody was mixed with 0.5mL of papain beads (Invitrogen) pre-equilibrated in 20mM sodium phosphate, 20mM EDTA, and 20mM fresh L-Cysteine, incubated at 37°C overnight with 20rpm rotating. Digested Fab and Fc were separated from the beads through gravity columns with substantial washings of 20mM sodium phosphate. The cleaved Fab and Fc mixture of cD9 was diluted 100× in 10mM Tris, pH 8.0 and separated by HiTrap SP HP column (GE Healthcare) in a gradient of 0M to 1M NaCl mixed with 10mM Tris, pH8.0. The eluted Fab was concentrated into 40mg/mL and stored at 4°C before crystallization or complex formation.

Alanine scanning of D9 antibody

The site-directed mutagenesis of the recombinant hD9 antibody construct was introduced by PCR. The mutant regions involve the heavy chain G26 to T33, I53 to T 58, R98 to Y106, and light chain S27 to Y31, D49 to S51, Q88 to T96 which were confirmed by DNA sequencing (Mission Biotech). The antibody mutants were expressed in 30 mL Expi293F cells by using ExpiFectamine™ transfection reagent (Gibco) following manufacture's instruction and were purified by Protein-A beads (GE Healthcare) as previously described. The purified antibodies were tested for binding to FG hIL-17RB ECD using ELISA and O.D 450nm was read by Multiskan™ GO Microplate Spectrophotometer (Thermo Fisher Scientific).

Structure modeling

The extracellular domain sequence of bovine IL-17RB, R18-G275, was structurally modeled at SWISS-MODEL (Waterhouse et al., 2018). The template of homologous model was based on the solved X-ray crystal structure of the Interleukin-17 receptor A (PDB ID: 3jvf.1.C).

Crystallization

IL-17RB was constructed from bovine source (Uniprot: A3KN55) to obtain higher expression in acetylglucosaminyltransferase I ($GnTI^-$) deficient HEK293S cells. The sequence identity between human and bovine IL-17RB ECD (18–267) is 78.4%. The purified bIL-17RB ECD protein was digested by Endo H to become the mono-GlcNAc decorated (MG) protein and mixed with antibody D9 Fab in a molar ratio of 1:1.5 for one hour at room temperature. The mixture was further purified by size exclusion column to remove the excessive D9 Fab. The final concentration was 15mg/mL for hanging-drop vapor diffusion at 20°C. The crystals of D9 Fab complexed with mono-glycosylated bovine IL-17RB ECD were grown in a drop of 1:1 ratio mixing with reservoir of 100mM Bicine (Molecular Dimensions), pH8.2, 17% PEG3350 (Molecular Dimensions) with 15μg/μL complex protein by Mosquito Crystal Robot (SPT Labtech) in 0.1μL per drop. Crystals were harvested at day 96 after being dehydrated by adding 0.2ul of reservoir and 0.1ul 50% PGE3350 into the drop, incubating for 10minutes, and then adding another 0.1ul 50% PEG3350 for 10minutes. Diffraction data were collected in synchrotron at wavelength of 1Å and processed by iMosflm (Powell et al., 2013).

Structure determination and refinement

The crystal structure was solved with space group $P2_1$ with four complexes packed in one asymmetry unit (ASU). The phase was solved by Phenix package using molecular replacement (Phenix.phaser-MR) (He et al., 2016). For IL-17RB, we used a modeling structure of bovine IL-17RB by SWISS modeling (Waterhouse et al., 2018), as searching template, which was separated into two parts of fibronectin domain 1 and 2 without the flexible linker region P143 to P165. The search model of D9 Fab was separated into four ensembles, including the variable region of heavy chain (VH; PDB: 4HJG) & light chain (VL; PDB: 4HJG) and constant region of heavy chain (CH1; PDB: 4KUZ) & light chain (LC PDB: 4KUZ). According to Matthews coefficient, there are four complexes in one asymmetry unit, with a solvent content of 42.01%. The refinement was accomplished by Coot (Emsley and Cowtan, 2004; Emsley et al., 2010) and Phenix.refine. The refinement strategies included XYZ coordinates, TLS parameters, individual B-factors, occupancies, NSC restraints and TLS (Afonine et al., 2012; Echols et al., 2014; Liebschner et al., 2019; Zwart et al., 2008). All structural figures were generated with UCSF ChimeraX (Goddard et al., 2018; Pettersen et al., 2021).

Phage-display library design for affinity maturation

The statistics of the nature prevalence was obtained from the human antibody database on abYsis of 164,119 human antibodies in 2016 (Swindells et al., 2017). The prevalence was listed as the percentage below each amino acid appearing on each CDR site by Kabat numbering system. The antibody library was designed to cover as many target diversities as possible and was limited to the adjacent region around D9 LCDR3, including LCDR1, LCDR2, and HCDR3.

Phage-display bio-panning for affinity maturation

The dsDNA containing phage-displayed libraries of HCDR3 alone (289ng/μL), LCDR1 alone (328ng/μL), LCDR2 alone (298ng/μL), and 3CDR combination (359ng/μL) were electroporated into TG1 component cells (Lucigen) in ice-precooled 2mm electroporation cuvettes. The electroporation energy was 2500volt, 25μF in exponential decay, and 200Ω resistance (Gene Pulser Xcell^{TM}, Bio-Rad). The TG1 cells were recovered in recover reagent (Lucigen) at 37°C, shaking 250rpm for 1 h, and then incubated on 24.5cm^2 large square plate (Corning) at 30°C overnight. On the second day, the part of library TG1 cells were resuspended in 25mL 2xYT containing 50μg/μL ampicillin and 2% glucose to grow to log phase. Then, TG1 cells were infected with 10 MOI of helper phage at 37°C, shaking at 100rpm for 30 min and then 250rpm for 30 min. Then 225mL 2xYT containing 50μg/μL ampicillin, 2% glucose, and 50μg/μL kanamycin was added for incubation at 37°C, 250rpm overnight. The supernatants containing phage-displayed library were harvested by centrifugation at 8000rpm, 20 min and added 50mL of PEG8000/2.5M NaCl at 4°C for one day to precipitate the bacteria phages. The phages were collected by centrifugation at 12000rpm, 20 min. And PEG8K/NaCl precipitation was repeated for twice. After purification, the phage was resuspended in 200μL PBS and incubated with Protein G Magnetic Beads (Thermo Fisher Scientific) precoated with hIL-17RB-Fc fusion protein for interaction. Three 0.05% PBST washings were applied to remove the nonspecific bindings. After wash, the Protein G bound with hIL-17RB_Fc_hD9 scFv complex was directly added into 10mL of log phase TG1 cells in 2xYT containing 50μg/μL ampicillin, 2% glucose. After incubation at 37°C, 250rpm for 1 h, the TG1 cells were centrifuged at 1500g for 12 min and resuspended into 20mL 2xYT containing 50μg/μL ampicillin, 2% glucose, and 50μg/μL kanamycin at 37°C, 250rpm overnight to generate the secondary generation phage-displayed library. The secondary generation library was used to repeat the interaction cycle via Protein G beads. The process was repeated for four to five times until the phage titer was starting to decrease.

Immunofluorescence

HEK293T cells were seeded on 0.17mm coverslips overnight in complete DMEM (Gibco) and transiently transfected with pTT_IL-17RB full length_EGFP using Lipofectamine (Thermo Fisher Scinetific) for three days. The cells were washed with 1xPBS once and then incubated in 200μL of MAXblock (Active Motif) for one hour. The cells then stained with 1:200 Cy5-labeled antibody 1B12 in PBS for two hours. After incubation, the cells were washed with 1xPBST (0.2% Tween 20) for three times and observed the fluorescence EGFP and Cy5 signals under Leica TCS SP8 (Leica).

Pancreatic cancer orthotopic mouse experiment

Eight-week-old NOD/SCIDγ female mice were injected with 2.5×10^5 GFP-LUC-tagged CFPAC-1 cells orthotopically. After one week, the size of tumor was examined by IVIS kinetics imaging system (Caliper Life- Sciences) and the mice were grouped anti-parallelly by tumor size. 5mg/kg of 1B12 antibody or control human gamma globulin (Jackson ImmunoResearch) was injected intravenously per week for four weeks. IVIS was used to monitor tumor growth and metastasis. To collect the result, tumors were weighed, and livers and lungs were examined for metastatic cancer cells. No criteria were set for including or excluding animals. And there is no animal excluded in this experiment. Statistical analysis was performed using two-tailed paired Student's t-tests.

QUANTIFICATION AND STATISTICAL ANALYSIS

All presented as mean ± SEM (Figures 1B and 1D and 5A and 6C). The significance of Figure 6C was determined by two-tailed paired Student's t-tests which is presented as $p < 0.001$ (***) indicated by asterisks.

Cell Reports, Volume *41*

Supplemental information

Structural basis of interleukin-17B receptor in complex with a neutralizing antibody for guiding humanization and affinity maturation

Wen-Hsin Lee, Xiaorui Chen, I-Ju Liu, Jiin-Horng Lee, Chun-Mei Hu, Han-Chung Wu, Sheng-Kai Wang, Wen-Hwa Lee, and Che Ma

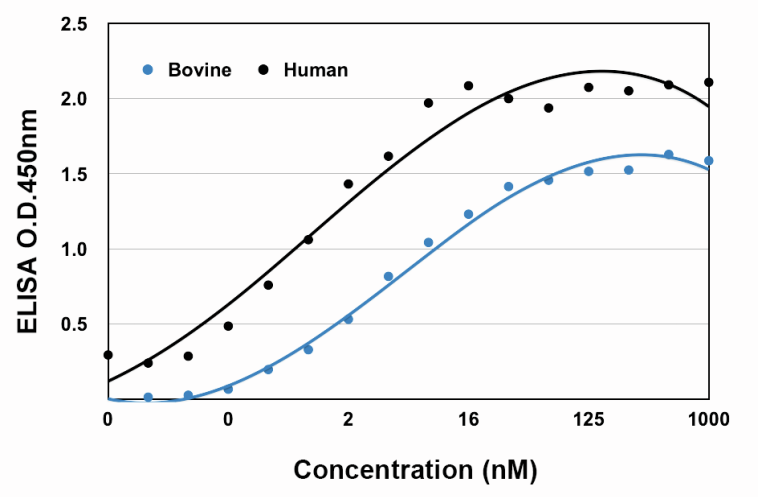

Supplementary figure 1. ELISA binding of mD9 toward human and bovine IL-17RB ectodomains, related to Figure 2. The ELISA plate was coated with human or bovine IL-17RB ECD protein. mD9 antibody was two-fold serially diluted. The result shows that binding affinity of mD9 to bIL-17RB (blue) is slightly weaker than hIL-17RB (black).

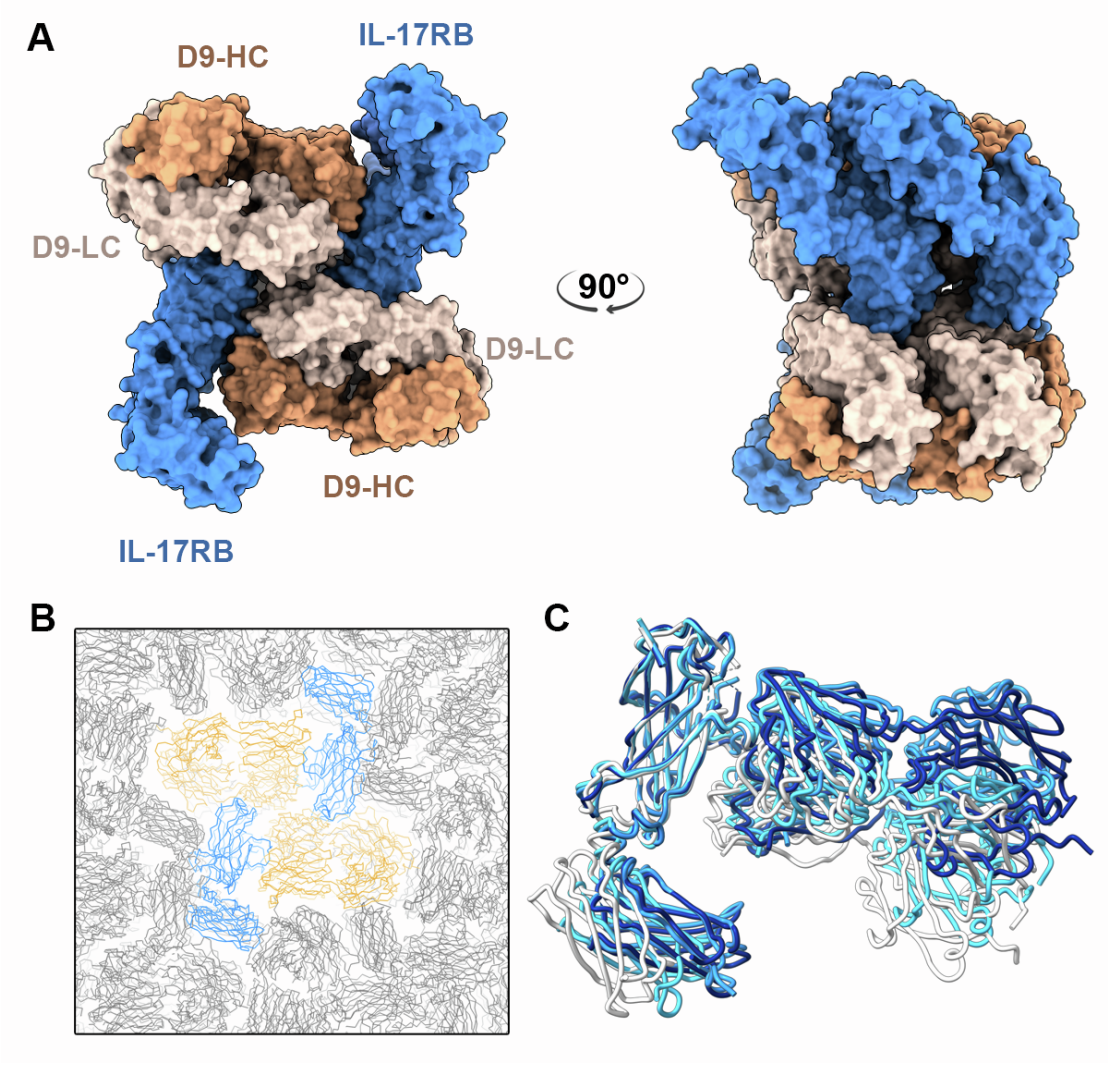

Supplementary figure 2. The asymmetric unit of bIL-17RB/cD9 complex structure, related to Figure 2.

(A) Four copies of the complex are found in one asymmetric unit , presented in two different view angles. IL-17RB colored in blue, Fab cD9 light chain in light orange and heavy chain in orange. **(B)** Crystal packing of the asymmetric unit (as shown in A) in the context of surrounding copies (grey), showing the crowdedness in packing. **(C)** The superimposition of four IL-17RB/D9 Fab complex copies in one asymmetry unit, focused on one FnIII domain only. The four complexes exhibit different angles between two FnIII domains and different orientations of the approaching antibody, without affecting the local interface. The angles between two FnIII domains are flexible and can be affected by the crystal packing.

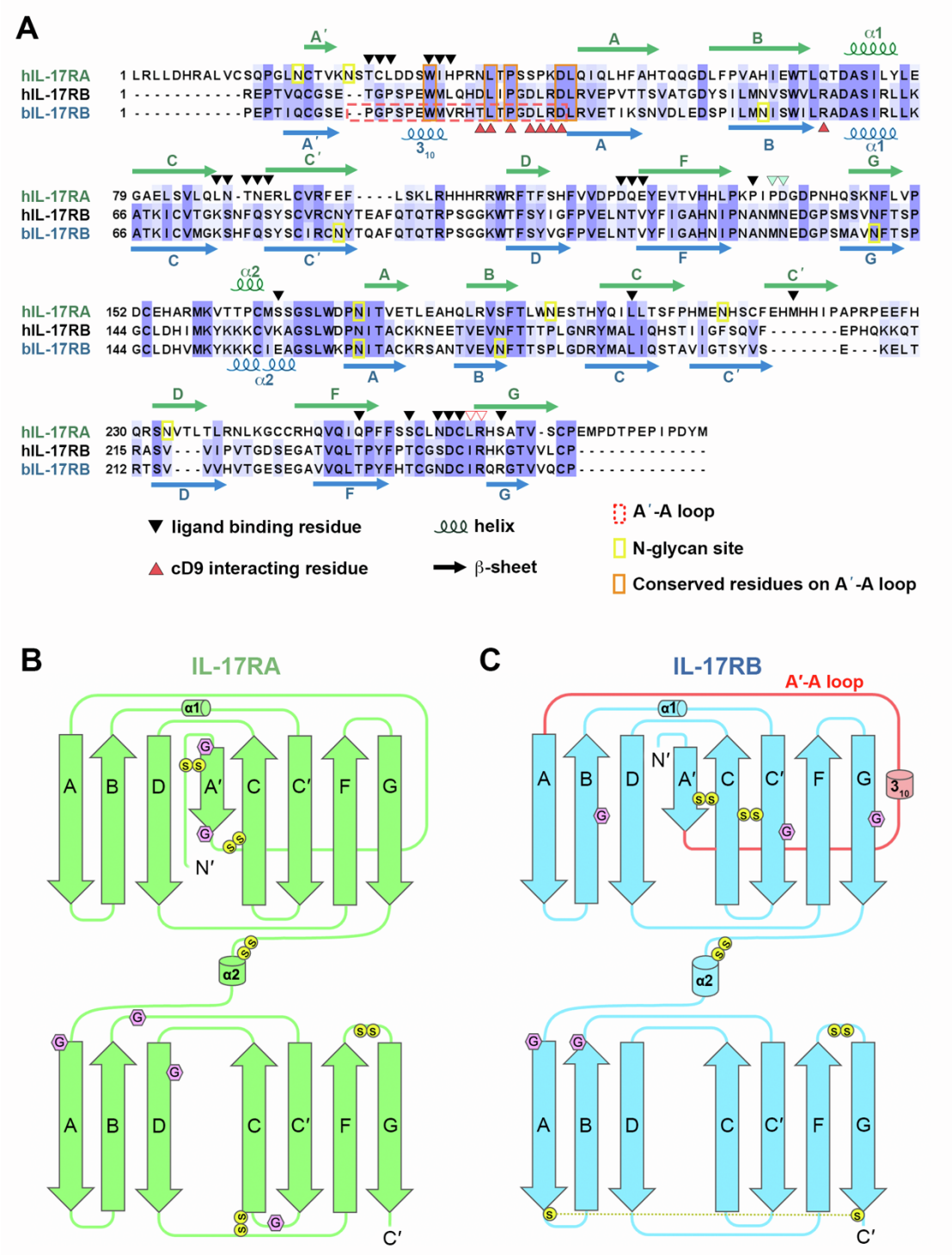

Supplementary figure 3. Sequence alignment the extracellular domain of human IL-17RA (hIL-17RA), human (hIL-17RB) and bovine IL-17RB (bIL-17RB), related to Figure 2.

(A) The sequences of hIL-17RA (UniProt: Q96F46), hIL-17RB (UniProt: Q9NRM6), and bIL-17RB (UniProt: A3KN55) are aligned by UniProt align tool (www. uniport.org), colored by percentage identity in a purple gradient. Darker color indicates higher conservation. The secondary structure elements of β-strands and α-helices are indicated with green (for hIL-17RA) and blue (bIL-17RB) symbols. Black triangles mark the ligand binding residues of IL-17RA and red triangles mark the cD9

binding residues. Yellow boxes mark the N-glycosylation sites. The A'-A loop of IL-17RB is framed in a red dashed-line box. Highly conserved residues in the A'-A loop are framed in orange boxes. **(B)** Topology diagram of the FnIII fold of IL-17RA. **(C)** Topology diagram of the FnIII fold of IL-17RB. The pink hexagons are N-glycosylation sites and the yellow circles are cysteines in disulfide bridges.

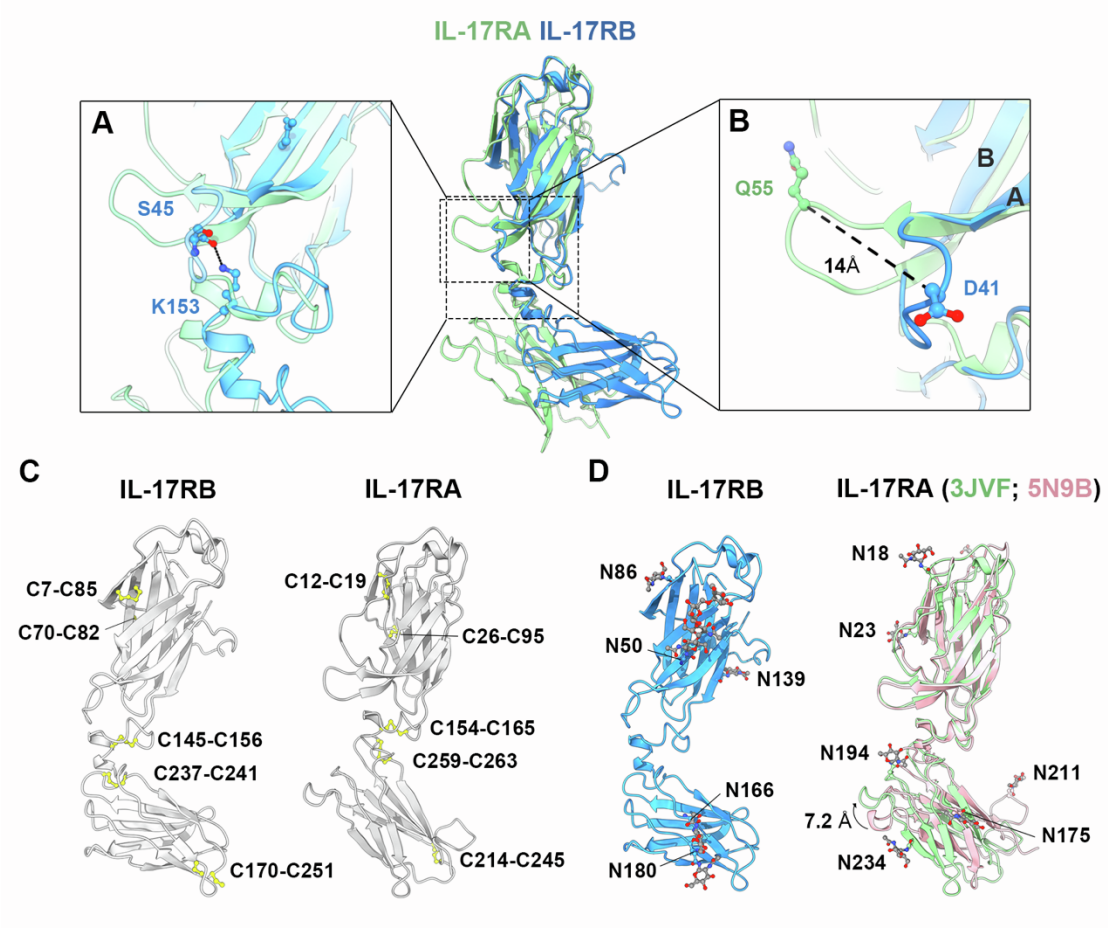

Supplementary figure 4. Structural comparison between IL-17RB and IL-17RA, related to Figure 2 and Figure 3.

IL-17RA (green) is superimposed onto IL-17RB (blue) shown as ribbons in the top middle with two enlarged views: **(A)** A hydrogen bond was observed between S45-O_γ on A-B loop and K153-N_ζ on the D1-D2 linker in IL-17RB, but not in IL-17RA; **(B)** The A-B loop of IL-17RB is ~14Å away from that of IL-17RA, measured by the distance between Cα atoms of corresponding residues (Q55/D41, Fig. S3A). **(C)** IL-17RB (left) and IL-17RA (right) are shown in the same view in white ribbons, with all disulfide bonds shown in yellow sticks and labeled. The C145-C156 and C237-C241 bonds of IL-17RA are structurally conserved in IL-17RB, but the others are different. Instead of holding adjacent β-strands, the disulfide bridges of C12-C19 and C26-C95 in IL-17RA D1 hold the N-terminal loop and the long A-A' loop close to the β-sandwich fold, while no such bonds are observed in IL-17RB to stabilize the A-A' loop. **(D)** IL-17RB (left, blue) and two IL-17RA structures (right, green and pink) are shown in the same view. N-linked glycosylation sites are labeled and glycans drawn in sticks. All the glycosylation sites harbor single GlcNAc residues in the mono-GlcNAc decorated IL-17RB, except for N50 which still has a Man-5 type glycan. Since some of the glycosites are mutated in IL-17RA (PDB 3JVF, green) and the unliganded IL-17RA (PDB 5N9B, pink) is used to show the rest of glycosylation sites.

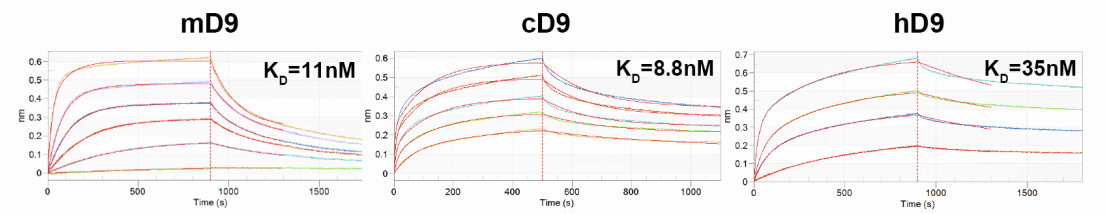

Antibody	Antigen	K_D (M)	K_D Error	χ^2	R^2	Rmax	Rmax Error
mD9	hIL-17RB ECD Fc-fusion	1.10E-08	4.6E-09	0.002	0.996	0.462	0.087
cD9		8.80E-09	4.9e-09	0.000	0.982	0.368	0.010
hD9		3.50E-08	8.6E-09	0.000	0.985	0.447	0.019

Supplementary figure 5. The kinetic binding curves of mouse, chimeric, and humanized D9 antibodies, related to Figure 5. Blue curves are the experimental trace obtained from biolayer interferometry (BLI), and red curves are the best global fit with 2:1 model to calculate the K_D in the summarized table. The K_D value of mD9, cD9, and hD9 are 11nM, 8.8nM, and 35nM, respectively.

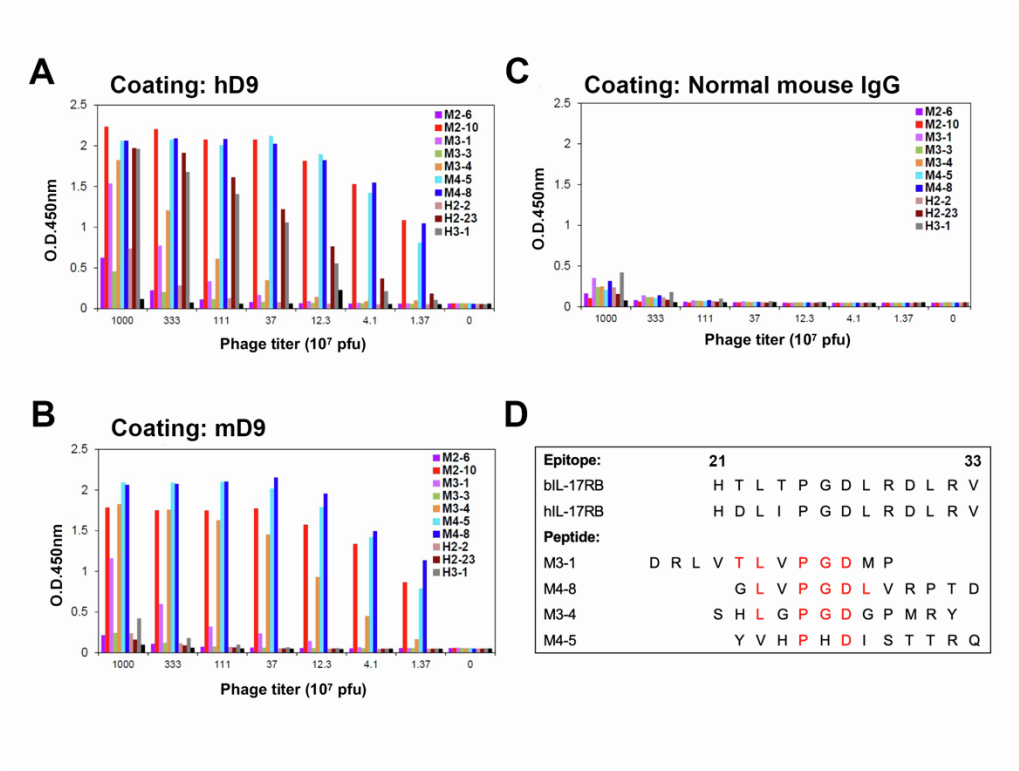

Supplementary figure 6. Human IL-17RB epitope mapping of mouse (mD9) and humanized D9 (hD9) via phage-displayed random peptide library assay, related to Figure 5.

(A-C) The ELISA plates were coated with hD9 (A), mD9 (B), or normal mouse IgG (C). The biopanning enriched phages carrying random peptides were applied onto the precoated ELISA plates in a gradient of doses (X-axis), and positive wells were sequenced with the pIII gene sequence of M13 phage. **(D)** Four of the random peptide sequences identified with dose-dependent binding in both hD9 and mD9 groups showed high similarity with the A'-A loop of both human and bovine IL-17RB (T/D22 to L28) which matched the epitope observed in the complex crystal structure.